



**University of
Reading**

UNIVERSITY OF READING

DEPARTMENT OF METEOROLOGY

**Impact of future climate change on extreme hot events
in the Maritime Continent region**

Yesi Sianturi

A dissertation submitted in partial fulfillment of the requirement for the degree of
Master of Science, Applied Meteorology and Climate with Management

August, 2018

Abstract

The frequency and severity of extreme weather events are expected to change in the future, and the Maritime Continent region is one of the regions that are highly vulnerable to this impact of climate change. In this study, the impact of climate change on extreme hot events over the Maritime Continent region is examined using in situ and gridded observations, in combination with climate model simulations.

Before being used in the projection, the GCM (global climate model) simulations are evaluated and adjusted to represent the observed extreme better and to remove potential biases between model simulation and the observation. The variance scaling method is used to adjust the statistical properties of the daily maximum temperature simulated by the GCMs closer to the distribution of the observed maximum temperature. Gridded observation is used to represent the current extreme temperature and to evaluate the climate model. Three extreme climate indices are defined, to assess the changes in the magnitude (TXx, or absolute maximum temperature) and the frequency (T90, percentile-based-threshold index, and T30C impact-based-threshold index) of extreme hot events, which are derived from the daily maximum temperature. To assess the changes of extreme hot event in the near future (up to 2050), the RCP4.5 scenario is used.

A significant increase of the frequency of extreme hot events is found in the 1981 – 2010 period over the Maritime Continent region. However, the absolute maximum temperature (TXx) does not show a significant increase in the regional average. Even after bias adjustment, the model simulations still cannot completely capture the pattern of warming over the Maritime Continent region and some biases exist between the simulated and observed indices. Biases found in the model evaluation are then used to interpret the projection of the extreme climate indices in the future period. The annual exceedance of T90 index will be increased by 55 ± 7 days in the 2031 – 2050 period compared with the 1986 – 2015 period. However, the model evaluation result implies that the real annual exceedance is expected to be higher than this value. The annual exceedance of T30C index is projected to increase by 41 ± 20 days in the 2031 – 2050 period compared with 1986 – 2015 period, yet, the high annual exceedance of T30C in the observation period (± 252 days in 1981 – 2010 period) implies that this index is no longer representative as an extreme-temperature index. The changes of the magnitude of the extreme hot events (TXx) are not conclusive. This study attempted to quantify the impact of future climate change to extreme hot events over the Maritime Continent region, however, various limitations are recognized and more thorough study is needed to make a more reliable analysis.

Acknowledgement

I would like to thank my supervisors, Professor Richard Allan and Rebecca Jones for their guidance, ideas, and support throughout this project, and to Dr Chun Lei Liu, for his technical help and insight during the dissertation writing process. I would also like to thank WMO (World Meteorological Organization) and UK Met Office for giving me the opportunity to continue my study in the UK. My gratitude also goes to my colleagues in Indonesian Agency for Meteorology Climatology and Geophysics for their kind support, prior to and during my study here.

Content

1. Introduction	
1.1 Background	1
1.2 Motivation	3
1.3 Objectives	3
2. Literature Review	
2.1 Weather and climate system over the Maritime Continent region	5
2.2 Temperature profile and causes of maximum temperature	7
2.3 Temperature extreme in Southeast Asia region	9
2.4 Extreme climate indices.....	13
2.5 Summary	15
3. Methodology	
3.1 Data	17
3.2 The causes of extreme hot event	20
3.3 Future climate Projection	21
3.4 Extreme climate indices	25
4. Drivers of Extreme Hot events	
4.1 Large scale driver of extreme hot events	27
4.2 Regional scale processes	31
4.3 Discussion	34
5. Current Hot Extremes and Model Evaluation	
5.1 Current hot extremes	36
5.2 Model evaluation	37
5.3 Discussion	44
6. Future Extreme Hot Events	
6.1 Projection of maximum temperature	48
6.2 Spatial distribution of extreme climate indices	40
6.3 Regional average of extreme climate indices	52
6.4 Projection of extreme hot event in energy planting site	55
6.5 Discussion	56
7. Conclusions	
7.1 Conclusion.....	58
7.2 Limitations and further work	59
8. References	61

Chapter 1

Introduction

1.1 Background

Anthropogenic climate change is projected to continue and alter weather pattern all over the world in the near future and beyond. Unprecedented changes have been observed in the last few decades, namely the warming atmosphere and ocean, the diminishing snow and ice cover, and the rising sea level (IPCC, 2014). Not only changing the mean state of the atmosphere, certain types of extreme weather are also expected to increase along with the underlying warming, particularly the ones that related to heating (Trenberth, 2012). In fact, climate change is often perceived by the changes in the frequency and severity of extreme weather events, as the extreme weather events have more tangible impacts on society. Extensive heatwaves, prolonged drought, record-breaking temperatures, often lead to detrimental damages to our functioning society.

In this study, the changes of the extreme hot event in the tropical region, the Maritime Continent region in particular, will be the main discussion. Given the low internal climate variability in the tropical region, even the smallest change in the mean system will result in a significant increase in the magnitude and frequency of extreme weather events, and the future changes are projected to take place much earlier in the tropical region than in the higher latitude region (Harrington et al., 2016). As the original climatic condition over the tropical region is hot and humid, the impact of high temperature events, or extreme hot events, will be more perceptible and will lead to more severe conditions. The smallest increase in temperature can potentially increase the heat stress to an intolerable level (Im et al., 2018). This region also consists of various ecosystems that resulted in a high level of biodiversity, and the warmer climate put this high level of biodiversity at risk (Mora et al., 2013a). The livelihood and economic activity of the inhabitants also depend on the ecosystem and the natural resources, hence, the projected warming climate threatens the economic sustainability in this region (Case et al., 2007). On top of that, most of the countries that exist over this low latitude region are developing countries, and most of those countries have lack of ability to adapt in the changing climate (Schiermeier, 2018).

Extreme weather events happen when the unforced natural variability favours the anomaly that amplifies the impact of the underlying warming (Trenberth, 2012). The temperature profile over

the Maritime Continent region shows small spatial and temporal variability, as there is a small variation in solar insolation throughout the year, and temperature profile is mainly affected by the physical processes between the ocean and the atmosphere (Li et al., 2017). Lying between two major oceanic regions, the main modes of variability of sea surface temperature (SST) over the Pacific and Indian Ocean, El Niño Southern Oscillation (ENSO) and Indian Ocean Dipole (IOD), become the main drivers of interannual variability over the Maritime Continent region. The occurrence of extreme hot events in this region is often linked with both modes of variability, and the previous findings show that the impacts are significant (Cheong et al., 2018; Tangang et al., 2007). Other smaller scale processes might also contribute to the occurrence of local extreme hot events in the Maritime Continent region, however, there is still not much thorough analysis about such processes.

The changes in the mean state of the atmosphere have been long-investigated, however, the changes in extreme events are relatively newly explored. Estimating the impact of climate change to the frequency and severity of extreme weather events is challenging, as the exact contribution of climate change has to be separated from the unforced natural variability (Otto et al., 2016). One of the main complications in assessing the changes in extreme events is the high resolution spatial and temporal observation that is required for the assessment, as the extreme weather events often occur locally (Cheong et al., 2018). Moreover, extreme events are largely statistical problem; the quality and consistency of observational data are also major problems in characterizing the extreme events. The fact that there is a small number of occurrences of extreme events in the historical period also make the analysis regarding extreme weather events often not statistically robust. To resolve these problems, several regional workshops for the Southeast Asia region were held in order to assess robust and seamless analysis of the changes in the extreme climate (e.g. Caesar et al., 2011; Griffiths et al., 2005; Manton et al., 2001). However, often a large part of the Maritime Continent region was excluded from the analysis due to data availability issue.

Whilst assessing the current extreme event is challenging, projecting the changes of extreme event in the future is even a much larger issue. Climate models are often used to project the climatic condition under different warming scenarios. However, projection shown by climate models are not designed to predict the correct timing of the unforced internal variability of the climate system (Risbey et al., 2014). Thorough evaluation of the climate models is needed to make it a reliable tool in representing extreme weather event. There are some efforts to utilize climate models in estimating the possible changes of extreme weather events in the future (e.g., Donat et al., 2013; Sillmann et al., 2013b) and some initial analysis were made. Continuous and detailed research is needed to make a useful analysis, and improvements are still made to date.

Even though ground observational data are often needed to make reliable analysis of the extreme weather event, several studies made use of gridded observation to assess the changes in extreme event, as gridded observational dataset as the regularly spaced observation is more practical to use in global and regional studies (e.g. Alexander et al., 2006; Yin et al., 2015). Gridded observation also has more consistent characteristic with climate model simulation, that the evaluation of models using the gridded observation can be done in a more straightforward way than using point observation (Haylock et al., 2008).

1.2 Motivation

Tropical regions are characterized by their small range of normal temperature; therefore, a small deviation caused by climate change could have a more significant impact in this region compared with the higher latitude region (Trewin, 2014). Both cold and warm extreme event will change in the future changing climate, yet extreme hot events have more notable impact in this region. Various aspect of life will be disrupted by the changes in extreme hot events, especially those regarding life safety and economic viability. Previous studies have shown that the increasing temperature and extreme events are already evident in the Southeast Asia and Maritime Continent region (e.g., Caesar et al., 2011; Supari et al., 2017); further analysis on how these events will change in the future will provide information required to make beneficial decisions.

Additional to those issues, one of the main motivations in this project is to analyse how the changes in extreme hot events will affect the infrastructure sector, particularly those related to energy production. Extreme hot events affect energy production sector in various ways; other than increasing energy demand in extreme hot events (for cooling system, for instance), extreme hot events can also reduce the efficiency in energy production process, and threaten the workforce safety in energy planting environment (Añel et al., 2017; Xu et al., 2009). Gas turbines are often used in the energy generation process, and the output and efficiency of those gas turbines largely depend on the ambient temperature (Kakaras, 2006). The impact on every gas turbine will be different, and the function between the ambient temperature and the efficiency is empirical (Farouk et al., 2013). However, an approximate threshold for any gas turbine in general can be estimated (will be discussed in Section 3.4). A particular gas power plant site exists in the Maritime Continent region (Figure 3.1), and some parts of the analysis in this study will be done while keeping this motivation in mind.

1.3 Objectives

This study aims to analyse the impact of future climate change on extreme hot events over the Maritime Continent region. Changes in the frequency of those extreme values are reviewed to

evaluate how extreme temperature event will alter in the changing climate. A first step is to develop a methodology to adjust climate model output to better represent real observed temperature, in order to increase the relevance of future climate model projection. Some extreme temperature indices are used to quantify the trend of the changes. In addition, the drivers of extreme hot events are briefly discussed, to give a better comprehension of the physical process that leads to an extreme event, and to understand the concept of possible changes of extreme hot events in the future.

Specific objectives include:

- Investigate the current characteristic of temperature extremes over the Maritime Continent region.
- Evaluate how the climate model simulation can represent the present day characteristic of observed temperature extremes.
- Investigate how the frequency and magnitude of extreme temperature event will change in the future.

The structure of this report will be as follows; chapter 2 contains literature reviews of general overview of climate over the Maritime Continent region, the pre-causes and current changing temperature extreme in the Maritime Continent region; chapter 3 contains a detailed description of methods used in this report; chapter 4 – 6 contain the results of the analysis; chapter 7 contains conclusions and direction for future work.

Chapter 2

Literature Review

2.1 Weather and Climate in the Maritime Continent Region

Maritime Continent is defined as the archipelago in the Southeast Asia region, spanning over the equatorial belt. The term Maritime Continent itself was coined by Ramage (1968), describing one of the three active convection centres in tropical region with distinctive orographic features. Maritime Continent region is bounded by mainland Asia in the north and Australia in the south and surrounded by two major oceanic regions, the Indian Ocean and Pacific Ocean. This region includes the archipelago of Indonesia, the Malay Peninsula, Papua New Guinea, and Philippine. There are five main islands over the Indonesian region, Sumatra, Java, Borneo, Sulawesi, and Papua. More than 200 million people live in this region – the population of Indonesia alone is 261.1 million (World Bank, 2018) – and this unique geographical condition yields a society that heavily depends on the weather and climate. The warm and humid climate also creates an appropriate habitat to a large number of species from diverse ecosystems, making it as one of the richest repositories of biodiversity (Case et al., 2007).

Given its position, various mode of variability and weather events in the surrounding region contribute to determining the weather and the climate system across different spatial and temporal scale. The substantial total coastline length in this region makes up 80% of the total earth's equatorial circumference (Yoshida et al., 2005), and the diurnal cycle that related to land-sea interaction becomes the main mechanism for convective activity over the Maritime Continent region, over the coastal region in particular. This diurnal cycle is then amplified by subseasonal, seasonal to annual, and interannual variability.

One of the main drivers of seasonal to annual variability over the Maritime Continent region is the Asian-Australian monsoon and ITCZ (Intertropical Convergence Zone). Both phenomena are driven by the relative movement of the sun and the difference of heat capacity between ocean and land, creating an asymmetric pattern of heating over tropical region. The convective centre is usually located over the area with maximum heating, and the general pattern of annual precipitation is strongly influenced by this annual cycle. Aldrian and Susanto (2003) divided the climatic type in Indonesia into three types, based on the seasonal pattern of precipitation (Figure 2.1). The type

A region is dominated by one peak annual rainfall season, following the southward movement of the sun. The type B region is marked with high precipitation throughout the year and two peaks of annual rainfall. The last type of the climatic condition in Indonesia (type C), is affected more by the sea current over the region. As Indonesian throughflow flows through the Maluku Sea, it brings the ocean current from the warm pool area. The seasonal pattern of sea surface temperature over warm pool determines the peak of precipitation in this region, leads to an inverse pattern of annual precipitation with the type A region (Aldrian, 2008).

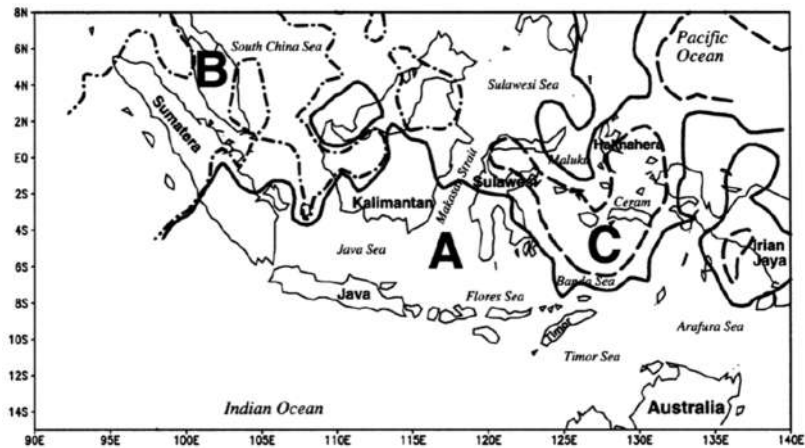


Figure 2.1 Three climatic region over Indonesia, based on precipitation pattern (Aldrian, 2003). Type A is the region with one annual rainfall peak (December – January), type B is the region with two annual rainfall peak (April and October), type C is the region with one annual rainfall peak (July – August).

The main interannual variability over the Maritime Continent region is driven by the sea surface temperature over the surrounding oceans, El Niño Southern Oscillation (ENSO) and Indian Ocean Dipole (IOD). ENSO is the coupled interaction between the ocean and atmosphere that characterized by an interannual oscillation of positive and negative anomaly of sea surface temperature in the tropical Pacific Ocean. IOD is an oscillation of sea surface temperature between the western and eastern tropical Indian Ocean, which affect the convective activity over the adjacent areas. The dry and warm condition over most of the Maritime Continent region is usually associated with warm ENSO event, meanwhile wetter condition is expected in La Nina condition (Harger, 1995), especially at the type A region. The impact of IOD is much less consistent over the region, but negative IOD events are often linked with positive anomalies of precipitation and the results are more significant over areas adjacent to the Indian Ocean (As-syakur et al., 2014; Nur’utami and Hidayat, 2016). In the intraseasonal timescale, Madden Julian Oscillation (MJO), an eastward moving cluster of cloud and rainfall near the equatorial region, often interacts with diurnal cycle in the Maritime Continent during the wet phase. MJO modulates the precipitation

variability within the seasonal timescale, in which the ascending region of MJO is associated with positive precipitation anomaly in the area underneath (Hidayat, 2016).

2.2 Temperature Profile and Causes of Temperature Extreme

The annual variation of sunshine duration and intensity over the Maritime Continent region is small given the low latitudinal position, which most of this region experiences almost the same length of day all year (approximately 12 hours). As the major determinant of the temperature profile, this small variation in solar radiation accounts for the homogeneous pattern of temperature over the Maritime Continent region. Hence, the diurnal variation of temperature in the tropical region is more prominent than the higher latitude. This is caused by the fact that there is an approximately same length of time between heating and cooling, that provides a balance between heating and cooling. In higher latitude region, the length of night (day) is too short in summer (winter) for effective cooling (heating). The high average temperature over the tropical region is also one of the main causes of strong diurnal variation, as the emission of heat is proportional to the fourth power of absolute temperature (Visher, 1922).

Complicated processes determine the temperature profiles over the Maritime Continent region. The high reception of solar radiation throughout the year makes this as one of the highest energy surplus regions, yet, then the intensive cloud cover often hinders the impact of this high radiation (Aldrian, 2008). The seasonal pattern of solar forcing affect the seasonal cycle of temperature over the Maritime Continent region (Figure 2.2) (Li et al., 2017), but there is an apparent lag between maximum solar insolation and warmest period observed, as the ocean stores the solar radiation energy and exert its influence to surface temperature later. Other dynamical processes and radiative processes between ocean and atmosphere also exert influence on the annual cycle such as the heat storage of the ocean and land, clouds, and latent heat flux in the surface. Li et al., (2017) studied the attribution of these processes in shaping the climatological pattern of temperature over the Maritime Continent region. The maximum heating in March – April is due to decrease in overall cloudiness over this area (coincides with East Asia summer monsoon to the north of the Maritime Continent) and increasing humidity (strong cross-equatorial flow), that adds up the effect of longwave heating and shortwave heating, while in September – October these surface processes contribute less and solar forcing acts as the main forcing. In contrast, the minimum in June – July is mainly attributed to the negative contribution of solar forcing and reduction in humidity, as there is moisture convergence over the north of the Maritime Continent region in this period (related with mature phase of East Asian monsoon).

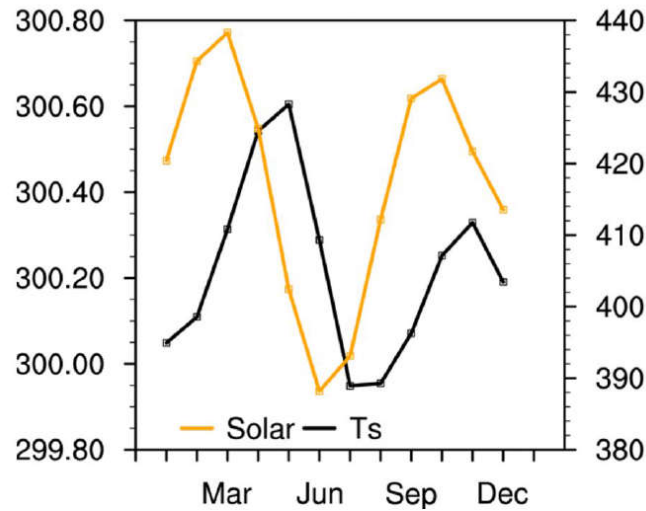
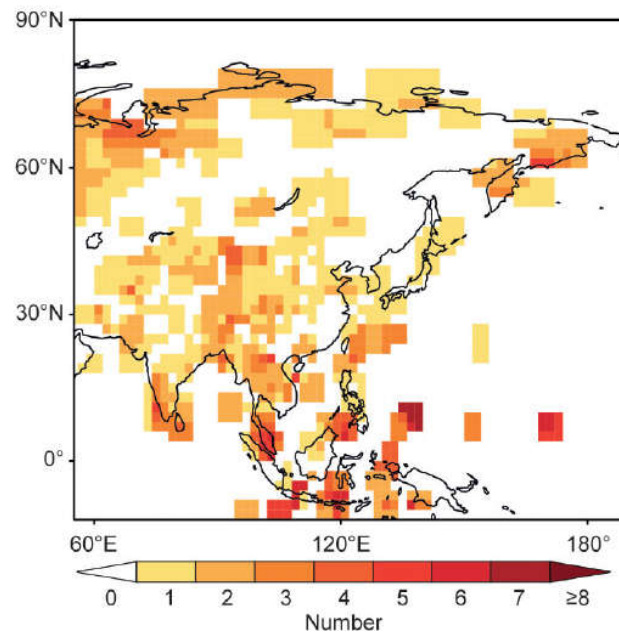


Figure 2.3 The annual pattern of solar insolation (yellow line) and surface temperature (black line) over the Maritime Continent region (Li et al., 2017). The left axis is temperature (K) and the right axis is the solar insolation (W/m^2).

Some sources of interannual variability can act to exacerbate the impact of the annual maximum heating over the Maritime Continent region. The existence of widespread precipitating clouds, particularly the ones that persist longer than the diurnal cycle, could potentially alter the temperature profile over the Maritime Continent region. Therefore, large-scale forcing that modifies the cloud distribution over the Maritime Continent region will also shift the temperature condition from its climatic average, which potentially can lead to extreme temperature events. Some modes of variability mentioned in the previous section, such as ENSO and IOD, will also affect the average temperature pattern.

The occurrence of strong El Niño is often related with high-temperature records in Southeast Asia region, that is mainly caused by the shift of deep convection centre, from the warm pool in the Western Pacific to further east in the Middle or Eastern Pacific (Halpert and Ropelewski, 1992). The troposphere over the Maritime Continent region is dominated by downward motion as a result of the weakening of Walker Circulation. The impact of El Niño to increasing global surface temperature, including Southeast Asia, seems to have a few months delay between both events, as the ocean current reallocate the heat when El Niño decays, in which the heat is transferred to the atmosphere as subsequent heating (Trenberth, 2002). As shown in Figure 2.2, the Maritime Continent region reaches its annual peak of surface temperature in April, and a recent attribution study found that El Niño contributes to the most extreme April temperature in Southeast Asia region, and this effect is exacerbated by the planetary warming (Thirumalai et al., 2017). In 2016, El Niño attributed to record-breaking temperatures in Asia including the Maritime Continent region for months (Figure 2.3), which the warming over the Maritime Continent region was driven

by the warmer Indian Ocean and subsidence over the Maritime Continent region (Imada et al., 2018).



*Figure 2.4 The number of warm month (monthly mean > 2*standard deviation, using 1951 – 2016 baseline) in 2016, related with El Niño 2015/2016 (Imada et al., 2018)*

Over the Indian Ocean, another mode of variability affects the temperature pattern over the western part of Indonesia in a similar mechanism with El Niño. The positive phase of IOD is usually followed with decreased precipitation over several regions in Indonesian Maritime Continent, meanwhile, the negative phase mostly accompanied by higher cloudiness instead. However, the impact of the positive phase is more pronounced over the dry season compared with the wet season, as the colder-than-normal sea surface temperature over the Maritime Continent during dry season amplifies the difference of the SST between the western and eastern side of the Indian Ocean. It is not as coherent as the impact of El Niño – the influence is mostly felt in the southern and eastern part of Sumatra (As-syakur et al., 2014). In some cases, positive IOD event coincided with an El Niño event, causing further reduction of precipitation and dryer condition than a single event, due to the much colder sea surface temperature over Indonesian Maritime Continent compared with both the Pacific Ocean and Indian Ocean (Nur'utami and Hidayat, 2016).

2.3 Temperature Extreme in the Southeast Asia Region

Using the output from various climate model simulations, the rate of warming over tropical regions is found to be smaller than the higher latitude region (Stocker et al., 2014). However, it cannot be said that the impact of this warming climate is going to be any more tolerable in the tropical region

(e.g., Im et al., 2018; Mora et al., 2013). Firstly, the changes in hot temperature extremes in the climate simulation are most robust over the tropical region (Harrington et al., 2016) (Hawkins and Sutton, 2009). This is because the internal variability, or the noise in the climate simulation for the tropical region, is lower than most regions in the world. Therefore, it can be implied that the signal-to-noise ratio for changes in temperature pattern is actually much higher in the tropic and these changes are more robust. In addition, the existing hot and humid climate over the Maritime Continent region makes the region susceptible to the smallest increase of temperature and the changes caused by such event will be unbearable (Im et al., 2018). On top of that, the socio-economic situation of the countries in the tropical region and its lack of capacity to adapt increase the vulnerability of this region to the climate change impacts (Harrington et al., 2016). As was mentioned before, the long-term planetary warming also potentially emerge faster in the tropical region, compared with any other region on earth (Thirumalai et al., 2017).

Despite the vulnerability and lack of adapting capacity of the countries in this region (Harrington et al., 2016; Pal and Eltahir, 2015), prior to the 21st century, only a few studies discussed the extreme climate events as the impact of climate change in the Southeast Asia region specifically. One of the main challenges in making such analysis was obtaining the data needed, as Southeast Asia region was considered as the area with bad meteorological record and the data was not freely available from the corresponding countries (Page et al., 2004). However, since the last few decades, the importance of assessing the changes in extreme weather events was recognized and some preliminary efforts including the international cooperation between countries in the Southeast Asia and Pacific region were done to address the challenges in making a continuous analysis. Recent studies regarding climate change impact to extreme climate events are summarized in Table 2.1, stating the participating countries in the study and the remarks compared to the previous studies (the remarks highlighted is only the remark on temperature analysis – those studies usually include both analyses on temperature and precipitation extreme). Some of the studies are using extreme climate indices in evaluating the changes in extreme climate events – this extreme climate indices will be discussed in the next section. However, it should be noticed that some regions are less inspected than the others, such as the Indonesian Maritime Continent, and those studies only discussed the observed changes on extreme climate events, but the simulation of how these changes will be continued in the future has not been explored much.

Study Conducted	Period of Analysis	Countries Included	Remarks
(Manton et al., 2001)	1960 - 1998	Thailand, Vietnam, Philippines, Myanmar,	This is the first study in the Asia Pacific region to

		Malaysia, Australia, Indonesia, Fiji, French Polynesia, Japan, New Caledonia, New Zealand, Papua New Guinea, and Samoa	analyse the extreme climate events, in a form of international workshop. This workshop then became the model for typical workshops in various countries.
(Griffiths et al., 2005)	1961 - 2003	Malaysia, Indonesia, China, Australia, Japan, Korea, Fiji, French Polynesia, Papua New Guinea, New Caledonia, and New Zealand.	The performance of mean temperature as a possible predictor for the changes in extreme temperature is examined. The correlation was high for tropical Pacific Ocean region, but much weaker over the continental region.
(Alexander et al., 2006)	1951 - 2003	Global analysis	Provide a seamless analysis of global extreme climate events. Similar to those regional studies, the widespread increase in maximum temperature was found. The gridded dataset was used.
(Choi et al., 2009)	1955 - 2007	Vietnam, Malaysia, China, Japan, New Zealand, Pakistan, Mongolia, Republic of Korea, Thailand, Australia.	Changes in extreme temperature event are less pronounced than the mean temperature, and the changes in warm events happened more rapidly compared with cold events.
(Caesar et al., 2011)	1971 - 2005	Vietnam Australia, Bhutan, Brunei Darussalam, Fiji, Cambodia, Timor Leste, Laos, Thailand, Maldives, Myanmar, Nepal, Sri Lanka,	Consistent results with previous studies using extreme climate indices were found, significant warming events,

			particularly warm night. The warm extremes are found to coincide with large El Niño event.
(Siswanto et al., 2016)	1866 - 2010	Indonesia (Jakarta)	The long-term analysis in Jakarta shows the effect of urbanization on extreme weather events.
(Marjuki et al., 2016)		Australia, Indonesia, Philippines, Singapore, Malaysia, Vietnam, Thailand, Cambodia, Myanmar, Laos, Brunei Darussalam, Timor Leste	The increase in night time temperature was associated with the crop field production.
(Cheong et al., 2018)	1972 - 2010	Brunei, Indonesia, Malaysia, Myanmar, Philippines, Singapore, Thailand, and Vietnam.	Stronger trends were detected due to the addition of new data. Climate model simulations are able to depict the observed trend well.

Table 2.1 Recent studies regarding extreme climate events in Southeast Asia.

Other studies regarding the observed and projected changes in extreme hot events and its sectoral impact were done to provide prior analysis of the significance of these changes to the functioning society. Using very high-resolution global model, Dosio et al. (2018) found that even in 1.5° C warming scenario, a portion of world population will be introduced to severe heat wave once every five years in average, including people in South East Asia region. A thorough study of projected climate change to heat-related mortality was done using four scenarios of climate change (Gasparrini et al., 2017). The overall impact of the changing climate is a significant surge in excess-heat-related mortality, while the impact of the cold event becomes relatively less important. Moreover, this general impact is much more prominent in the tropical region than the temperate climate region, and this becomes a crucial issue considering the number of population living in this region.

In the energy sector, the climate change issue is often related more to the generation of renewable energy sources, however, the increase in mean and extreme temperature will also affect energy sector in other various ways, such as changing the energy demand for certain season and disrupt the energy production of conservative energy sources (Añel et al., 2017). The ambient temperature determines the efficiency, longevity and workforce safety in oil and gas production facilities. In LNG (Liquefied Natural Gas) production, changes in the ambient temperature and surface pressure influence the cooling system that reduces the efficiency in energy planting process, and the size of the compressor is determined by the ambient temperature (Farouk et al., 2013; Bukowski et al., 2016). For a region that highly depends on its agricultural sector, the future warming climate will introduce great losses in the economy of these countries due to the decreases of production of the main agricultural commodity, such as crop (Marjuki et al., 2016; Zhai and Zhuang, 2012). The rising mean temperature will also have consequences on precipitation intensity as the water holding capacity of the atmosphere will increase in the warmer climate based on the Clausius-Clapeyron relation (Trenberth, 2011), and this will potentially establish more substantial impact as precipitation pattern holds a crucial role in the livelihood in this region.

2.4 Extreme Temperature Indices

As extreme climate events have direct impacts on society, extreme events definition and calculation have to be determined as carefully as possible. The persistence and occurrence of the event have to be considered to assess the possible impact of socio-economic activity. The efforts to assess extreme climate events are generally accomplished in two ways, by evaluating the return period of an extreme value using extreme value distribution analysis (Kharin et al., 2007; Wang et al., 2013), or by calculating the number of days a threshold is exceeded, also known as extreme climate indices (Klein Tank et al., 2002; Vincent and Mekis, 2006). While the first method reflects the extreme climate events that occur in several years or decades period, the latter method provides insight on extreme climate events that happen several times in a year or in a much shorter period. However, one of the main advantages of using extreme climate indices is its relatively more frequent occurrences, as it is more statistically robust to identify extreme-related-changes (Wang et al., 2013). Therefore, the application of extreme climate indices is more commonly used in evaluating the changes in extreme climate events. Folland (1999) formulate several desired characteristics for indices to assess the climate extremes:

- The ability to detect trend (signal) from one period to the other, instead of noise.
- Relevance to societal impact.
- Sensitivity to changes induced by either natural variability or anthropogenic factor.
- Can still be valuable when defined spatially over a wide area.
- Possible to compute using both observation and model data.

Choosing a suitable threshold or indices can be complicated, as there should be a balance between impactful events and statistical robustness, as estimation of the threshold is subject to sampling uncertainty (Zhang et al., 2011, 2005). Percentile based threshold, for instance, even though its number of exceedance in the base period can be predicted accurately (the percentage of exceedance for percentile 90 is 10%, by definition), but this exceedance rates outside the base period will be different, resulting in “step changes” between the start and end point of the base period and the effect of this “step changes” can significantly affect the trend calculation. A higher percentile index will be more prone to this step change, as the exceedance value of higher percentile index is much smaller and more exposed to the sampling problem.

It is also complicated to interpret changes in climate extremes, as daily data with good records are needed. Daily data are available in digital format in some regions yet, however, the efforts to preserve climate data in South East Asia and the South Pacific region were considered insufficient (Page et al., 2004). In addition, raw data of temperature and precipitation are simply not accessible from some countries for various reasons. This then adds the difficulties in making thorough extreme climate analysis in these regions.

To address those challenges, the efforts to create seamless analysis on climate extreme was discussed in CCI (Commission for Climatology)/ CLIVAR (Climate Variability) meeting in 1999, which lead to the formulation of a list of simple indices derived from daily temperature and precipitation with guidance on how to use them in terms of maintaining continuous analysis over a wide area. The idea of ETCCDI (Expert Team on Climate Change Detection and Indices) is to accommodate an international coordination of the development of climate extreme analysis and to use the specifically designed extreme climate indices to make a seamless analysis of extremes across countries. To afford the seamlessness, user-friendly software packages are made available for the international research community, using R and Fortran Language. In total, there are 27 indices of extreme climate events that are related with temperature and precipitation and the detailed definition can be found in http://etccdi.pacificclimate.org/list_27_indices.shtml.

In using the software packages, the quality of the data has to be evaluated for its quality and homogeneity. Some statistical tests are done within these software packages as well (Peterson, 2013). This includes some logical quality controls (minimum temperature should not be larger than maximum temperature, temperatures that are above unreasonable values), outlier detection, and missing data calculation. The rounding problems and duplicate dates that might be caused by different observation procedure in different countries can also be detected by running the extra quality control analysis (Zhang and Yang, 2004). However, to truly maintain the quality of the

data, local expertise is needed as the problem in the data might be unique to certain countries or local region.

2.5 Summary

The Maritime Continent region consists of thousands of islands, several countries, and a big number of the world population lives inside the region. A broad range of ecosystem and natural resources exists inside this region, creates a society that highly depends on the weather and climate system. There are some main modes of variability that affect the weather and climate system over this region, such as the Asian-Australian monsoon, ENSO, IOD, and MJO. Over this region, the temperature variability is more prominent in its diurnal cycle, compared with its annual cycle (Visher, 1922). The main forcing to the annual cycle is the solar forcing, even though some local dynamical processes also play crucial roles (Li et al., 2017). The complicated processes generate a pattern in which the regional temperature reaches the highest temperature in April, followed by the second peak in October. The lowest monthly temperature is shown in June – July, which is attributed to the lack of solar forcing during that period. Some large-scale processes are often associated with the extreme temperature event over the Maritime Continent region, particularly the extreme hot events, such as strong El Niño events and positive phase of IOD.

Due to its low internal climate variability, Southeast Asia region, particularly the Maritime Continent region, is prone to the changes in the mean state of the climate system. The impact of the climate change on this region is projected to be robust and will emerge sooner than any other region on earth (Harrington et al., 2016; Hawkins and Sutton, 2009). Changes in extreme climate events are detected and are expected to continue in the future. International workshops are held as the regional scale effort to create seamless analysis of the changes of extreme climate events related to the observed climate change, however, any attempt to project the changes of extreme climate events in the future period has not been initiated yet (e.g. Choi et al., 2009; Manton et al., 2001). In those workshops, extreme climate indices are used to evaluate the observed changes in extreme events, based on the various definition of extremes. In the following chapters, the changes of extreme hot events will be assessed, both in the observational period and in the future period.

Chapter 3

Data and Method

This chapter will contain a description of the region of interest, the observational data, global climate model simulation that will be used to assess current and projected extreme hot events, and the processes to prepare the data for the analysis. The analysis methods that will be used to answer the questions in the first chapter will also be discussed.

In brief, the methods used in this study can be described as follows. For the first part of the analysis, the drivers of extreme hot events will be discussed. The analysis will be divided into two, the large-scale weather patterns that cause extreme hot events, and the regional scale processes. The large-scale weather pattern that will be discussed are ENSO and IOD events, and case studies will be used to investigate the regional scale processes that might affect the temperature characteristic. This evaluation is meant to be a brief overview, instead of an exhaustive study of the drivers of extreme hot events.

For the second part of the analysis, gridded temperature from Berkeley dataset will be used to represent the observed extreme event over the Maritime Continent region, based on extreme climate indices defined in this study. The same extreme climate indices will also be calculated from all model simulations. However, the simulations need to be bias-corrected first to remove potential bias between the simulated temperature and the observed temperature. The gridded observation will also be used to evaluate climate model simulations, by comparing the trend of the extreme climate indices and maximum temperature in the observation period. The evaluation will be done by assessing the spatial distribution of the trend simulated and by comparing the trend of the regional averaged values, for all extreme climate indices and the maximum temperature.

For the last part of the analysis, the climate model simulation will be used to project the maximum temperature and extreme climate indices in the future period. The evaluation result from the previous analysis will be used to interpret the projection. An evaluation of how extreme hot event will change in the future and affect the energy planting site mentioned in Section 1.2, will also be done in this chapter.

3.1 Data

3.1.1 Region of Study

The region of interest in this study is the Maritime Continent region, here defined as the area within 10° S – 10° N and 90° E – 150° E. This consists data from nine countries which spread amongst thousands of islands. Large ocean areas are also included in this region, which affects the physical processes that shape the weather pattern over this region (Hendon, 2003). However, the analysis will be focused on the extreme hot events over land only, as the extreme hot events over land have a more direct impact to the society. In parts of this study, some of the analysis will be inclined more to the Indonesian Maritime Continent and its five main islands, as the whole country occupied most of the region of study.

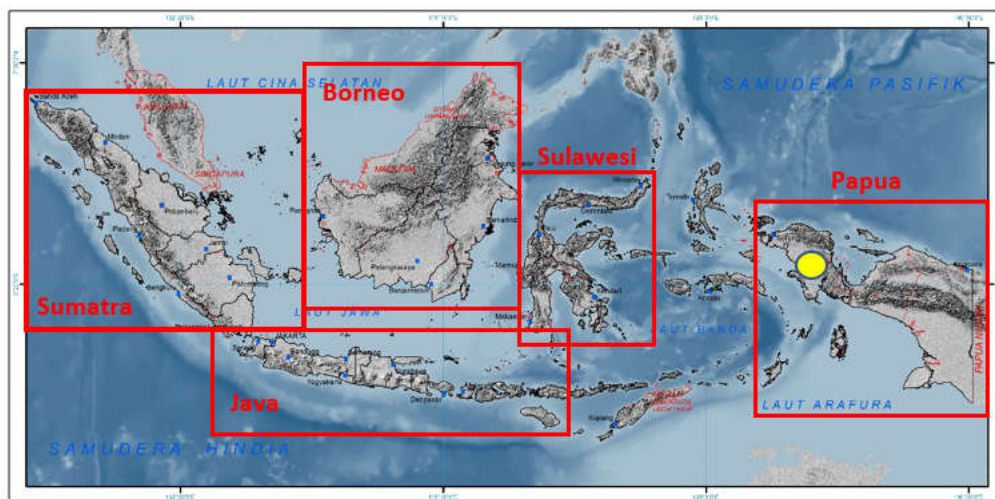


Figure 3.1 Region of Study. Darker shade (over land) indicates highland. Five main islands over Indonesia region are Sumatra, Borneo, Java, Sulawesi, and Papua. The yellow point is the location of gas turbine power plant site (source: BMKG).

3.1.2 Gridded Observation

In spite of being an area-averaged value of real observations, gridded dataset has some advantages compared with point observations, due to its regularity and consistency with climate models. The regularly spaced observations are preferable in various analysis, such as climate change impact analysis, as long time series needed and area-averaged-value gives a convenient solution to missing data issues. Gridded data can add some level of uncertainty due to the uncertainty in the station data itself and the interpolation method used to derive the area-averaged value (Hofstra et al., 2009). The number of density of the observation in each grid will also potentially add bias, as high density observation is represented more and grid data show closer value with the observation, yet biases are found as the number of observation in a grid decreased (Gervais et al., 2014). However, the

gridded observation can potentially reduce the uncertainty in the analysis instead, which is the uncertainty that comes from inconsistent station data, as quality control processes are applied in the gridding process and hence becomes a more robust method to use in climate change study (Yin et al., 2015). As models are generally more consistent with area-averaged value than point observation, a gridded observation also becomes an appropriate tool to validate climate models (Haylock et al., 2008). The ideal situation in climate change impact study is to use quality-controlled station temperature. Nevertheless, gridded observation provides consistent dataset and has an advantage regarding evaluating climate models. Taking that into consideration, gridded observation will be used to represent extreme hot events and to evaluate climate model simulations in this study.

The variability in the temperature pattern and current extreme hot events will be represented using gridded daily maximum temperature from the Berkeley dataset. The Berkeley gridded dataset is a gridded reconstruction of ground observation of temperature that using long temporal record (from 1701 – present) and includes large number of stations (approximately 39.000 records), combined from 16 existing archives, with additional ocean data from HadSST3 (Hadley Centre SST data set), with 1° X 1° resolution (NCAR, 2015). In this dataset, the utilization of such amount of observation was made possible by reducing the requirement of comprehensive record length to create a baseline, without losing the accuracy (A. Muller et al., 2013). The data has been quality controlled to remove outliers and inconsistent data, in addition, further mathematical techniques were applied to remove inhomogeneities in the series. As was discussed in section 2.4, the homogeneity assumption is crucial to extreme event analysis. Therefore such processes create a suitable dataset for extreme event assessment. In this study, the Berkeley gridded dataset is obtained from KNMI (Koninklijk Nederlands Meteorologisch Instituut) climate explorer (<https://climexp.knmi.nl/>).

To represent current extreme, the daily maximum temperature from the land area in the Maritime Continent region will be plotted, and extreme climate indices will be calculated from this dataset. To get an overview on how gridded dataset represents station observation, the skill score of daily mean temperature from gridded Berkeley and temperature from 134 stations in the Maritime Continent region is calculated and plotted in Figure 3.2. Skill score, as was described in Terando et al., (2012), is usually used to verify forecast skill, and can be used to measure the closeness of two sets of data, based on its correlation and standard deviation. The ground observation dataset was obtained from GHCN (Global Historical Climatology Network), and the period used for the calculation is from 1995 – 2017, based on the longest availability data from all 134 stations. From Figure 3.2 (a) and (b), it can be seen that on most stations, the skill score calculated is higher than 0.7 (1 is the maximum score). The imperfect relationship can be expected from the averaging method and quality control process, but such processes affect precipitation series more than temperature (Sun et al., 2014). The skill score is defined as (Terando et al., 2012):

$$S = \frac{4(1+r)}{(\hat{\sigma}_g + 1/\hat{\sigma}_g)^2(1+r_0)}$$

S = the skill score

r = Pearson correlation coefficient

$\hat{\sigma}_g$ = standard deviation of model normalized by standard deviation of the observation

r_0 = maximum attainable correlation, set as 1.

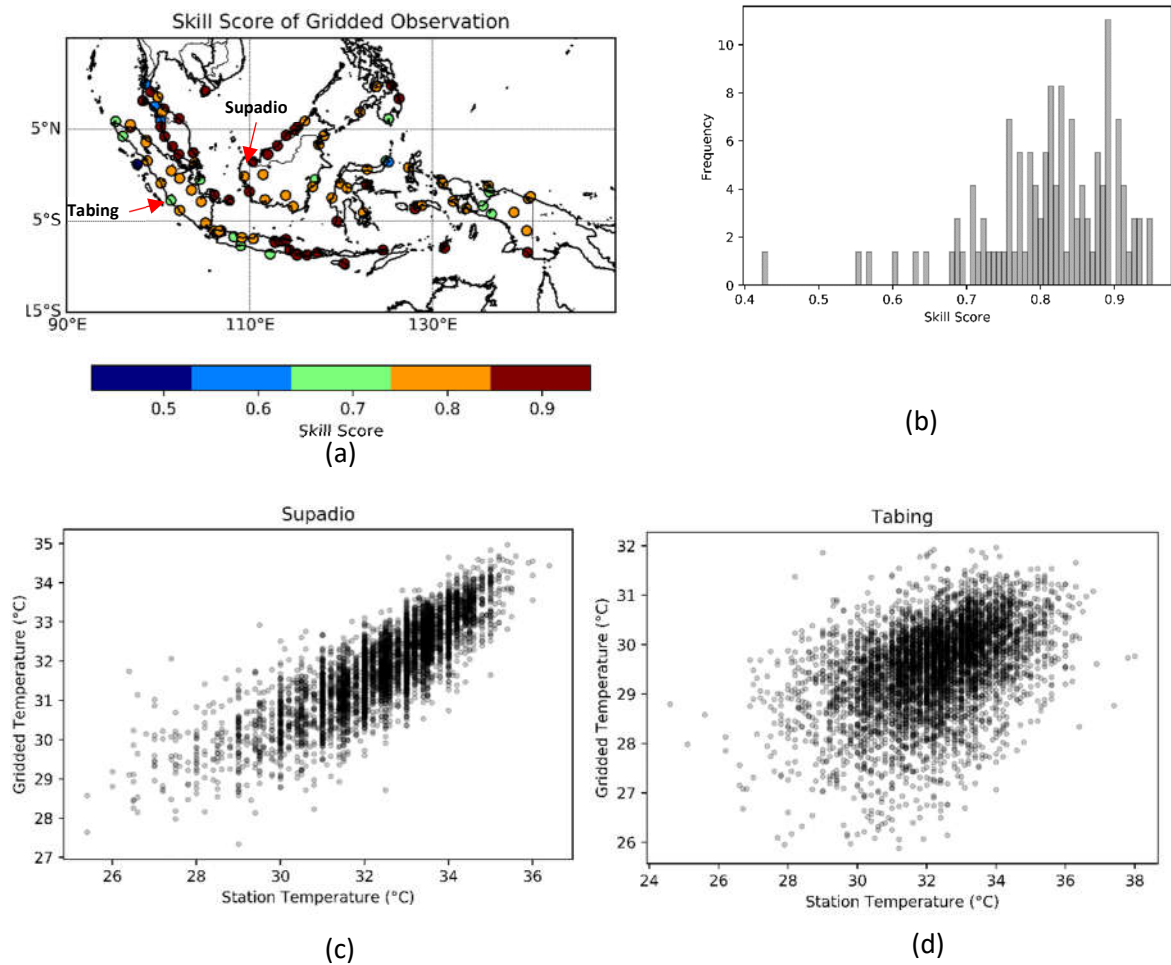


Figure 3.2 (a) Skill score of the gridded temperature Berkeley in representing daily maximum temperature in every station, (b) distribution of the skill score, (c) daily maximum temperature of gridded Berkeley and station observation in Supadio, (d) daily maximum temperature of gridded Berkeley and station observation in Tabing,

Daily maximum temperature series in two stations (Supadio and Tabing, Figure 3.2a) are derived from gridded temperature Berkeley and station observation and plotted in Figure 3.2 (c) and (d). For Supadio station, daily maximum temperature from gridded Berkeley is more closely related (r

= 0.83) with station observation, however, 1° C increase in station observation is followed by 0.6° C increase only in gridded Berkeley dataset (slope = 0.6). For Tabing station, the spread of the scatter plot is larger, indicates a weaker relationship ($r = 0.45$) between gridded Berkeley and station observation, and the slope is even smaller (0.25). This shows how the performance of gridded temperature as an alternative to real observation vary from one location to others. As was mentioned before, such differences might arise from the averaging process and the quality control processes to remove outliers and maintain homogeneity. In this study, no such bias adjustment is made between station observation and gridded observation, to avoid introducing inconsistencies in the gridded observation. However, the fact that gridded observation is not fully representing station observation will be used in concluding the results.

3.2 The Causes of Extreme hot events

Sillmann et al. (2017) highlights the main aspects that cause extreme weather event in a region; a large-scale driver that favours the occurrence of unusual weather pattern; an initial condition, such as unstable atmosphere or dry surface condition, that trigger the feedback processes; and a feedback, such as convection or the interaction (of land) with atmosphere. In this study, the possible large and regional scale drivers will be examined to understand the physical causes of extreme hot events in the Maritime Continent region. As the warm phase of ENSO (El Niño) and the positive phase of IOD are often linked with the dry and warm condition in the Southeast Asia region, both events will be examined in the first part of the analysis.

3.2.1 ENSO and IOD Indices

To define the periods with warm phase ENSO and positive phase IOD, two indices of SST anomaly over Pacific and the Indian Ocean will be used. For the warm phase of ENSO events (El Niño), the NINO3.4 index, the standardized SST anomaly over Nino 3.4 region, is chosen. This metric is the most used metric to assess ENSO impact over the Maritime Continent region, and in this study, the NINO3.4 index is obtained from <https://www.esrl.noaa.gov/>. For positive IOD events, the SST anomaly between western (60°E – 80°E, 10°S - 10°N) and eastern (90°E - 110°E, 10°S - 0°S) equatorial Indian Ocean, DMI (Dipole Mode Index), will be used. The DMI index is obtained from the same source. The definition for the phases will be:

NINO3.4	Category (El Niño)
0 – 0.9	Weak
1 – 1.4	Moderate
1.5 – 2	Strong
> 2	Very Strong

(a)

DMI	Category (IOD)
< -0.4	Strong Negative
-0.4 – 0.4	Normal
> 0.4	Strong Positive

(b)

Table 3.1. Intensity definition for ENSO and IOD events (source: BMKG).

3.2.2 Reanalysis Dataset

In the second part of the analysis, case studies of extreme hot events will be discussed to provide general information on the physical causes of extreme hot events in the Maritime Continent region. To reconstruct the meteorological conditions in that case, several weather parameters will be considered using the reanalysis dataset. Reanalyses is a “retrospective analysis” of the atmosphere, produced by assimilating observation data from various sources, including ground observation, satellites, ships, and aircraft, with the output of NWP (Numerical Weather Prediction) models, to develop an exhaustive record of weather and climate parameters (Parker, 2016). Reanalysis datasets are suitable to recreate the meteorological condition needed in this study, as it provides dynamically consistent data of various variables to best represent the real state of the atmosphere (Dee et al., 2016). The ERA-Interim reanalysis dataset used in this study is from ECMWF (European Centre for Medium-Range Weather Forecast) in which the spatial resolution is approximately 80 km, for a wide range of vertical levels, ranging from surface up to the 0.1 hPa level. The variables that will be considered are surface pressure, precipitation, wind, and soil moisture. Five most extreme events in a particular area will be listed, and the weather conditions that are suspected to cause such events will be examined.

3.3 Future Climate Projection

3.3.1 Global Climate Model

Climate models are the main tool to make future projections of climate, based on fundamental physical processes in the climate system. Even though extreme weather events are usually temporally and spatially local and challenging to depict with the coarse resolution global climate model, the available global climate models are found to represent extreme temperature events reasonably well (Kharin et al., 2005; Vavrus et al., 2006). In this study, six global climate models from CMIP5 (Coupled Model Intercomparison Project Phase 5) will be used to project the

maximum temperature and extreme climate indices over the Maritime Continent region. The six climate models used are listed in Table 3.1.

Model	Resolution (Lat X Lon)	Institution
HadGEM2-ES	1.25 X 1.875	Met Office Hadley Centre (MOHC)
CanESM2	2.79 X 2.81	CCCma (Canadian Centre for Climate Modelling and Analysis)
CNRM-CM5	1.40 X 1.41	CNRM (Centre National de Recherches Meteorologiques, Meteo-France, Toulouse, France)
GISS-E2-R	2 X 2.5	NASA/GISS (Goddard Institute for Space Studies)
MRI-CGM3	1.125 X 1.125	MRI (Meteorological Research Institute, Tsukuba, Japan)
BCC-CSM1.1	2.77 X 2.81	Beijing Climate Center, China Meteorological Administration

Table 3.1 Six Global Climate Model used in the analysis (ENES, 2018).

MRI-CGCM3 is a part of MRI ESM1 (Meteorological Research Institute's Earth System Model). It is comprised of three components which are the ocean-ice models, aerosol, and atmosphere-land, in which the atmospheric component is coupled with an aerosol model to capture the effect on the microphysics of cloud. This model was proved able to simulate near-surface temperature in the pre-industrial period and represent the overall climate of current period realistically, including some internal variability such as ENSO and both Antarctic and Arctic Oscillation (Yukimoto et al., 2012). CanESM2 is an earth system model that combines the atmosphere-ocean GCM CanCM4 and the land-atmosphere carbon exchange model, CTEM (Canadian Terrestrial Ecosystem Model). HadGEM2-ES is a part of the HadGEM2 project, which is the model that combines atmosphere-ocean coupling and earth system component, with improvements in atmospheric chemistry and the vegetation distribution (Collins et al., 2008). CNRM-CM5 is an earth system model that combines five models for atmosphere, ocean, sea-ice, surface, and river-routing scheme, which provides a better representation of near-surface temperature compared with its predecessor (Voltaire et al., 2013). GISS-E2-R is a part of the GISS (Goddard Institute for Space Studies) ModelE2, which is the atmospheric model that is coupled with the high-resolution dynamic ocean model (Schmidt et al., 2014). One ensemble from each model (mostly the first ensemble, r1i1p1, except for the GISS-E2-R) will be used to simulate the daily maximum temperature and extreme climate indices in the observation and future period.

Two simulations from each climate models will be used in this study; the historical experiment that applies realistic radiative forcings since 1850 to coupled simulations; and the RCP4.5 simulation, which is the continued historical simulations into the future by applying emissions to a stabilized radiative forcing at 4.5 Wm^{-2} in 2100. The evaluation of climate model simulations will be done in the historical period by comparing the trend simulated by climate models with the trend calculated from the gridded observation. All six global climate models will be used to project the maximum temperature to the near future period, up to 2050. Here, the application of one scenario only is based on the assumption that shorter term climate projection exhibits the modest sensitivity of climate change scenarios (IPCC, 2014), hence, the mid-level scenario is chosen in this study.

In evaluating the models (Section 5.2), comparison of trends is used instead of comparing the exact value of the simulation. This is mainly because the global climate models are not designed to predict the exact phase of the unforced natural variability (Risbey et al., 2014), therefore, comparing trends gives more reliable evaluation instead of comparing the exact value.

3.3.2 Bias Correction Method

In examining future climate change impact or extreme events, potential systematic biases in climate model simulation from the observation is a challenge, as extreme and impactful events depend on how realistic climate models represent real climatic condition (Smitha et al., 2018). Model biases might arise as an overestimated warming when used in simulating climate change, particularly in warmer and wetter climate (Christensen et al., 2008). In this study, a three-step bias correction method called variance scaling method will be used to remove potential biases in climate model simulations, using the mean and variance of the observation time series in the historical period. The complete calculation step was described by Teutschbein and Seibert (2012). The variance scaling method exhibits better performance compared with the linear-bias-correction method, however, as the main problem in using bias correction methods, the model projection will also be corrected using the statistical properties of observation in the observation period, which is assumed to be stationary in the future period (Teutschbein and Seibert, 2012). The variance scaling method is calculated using these three steps:

$$T'_i = T_{i,m} + \mu(T_{i,o}) - \mu(T_{i,m})$$

$$T''_i = T'_{i,m} - \mu(T'_{i,m})$$

$$T^* = T''_i \cdot \left[\frac{\sigma(T_{i,o})}{\sigma(T''_i)} \right] + \mu(T'_i)$$

which:

$\mu()$ = monthly mean of the quantity inside the bracket;

$\sigma()$ = monthly standard deviation of the quantity inside the bracket;

$T_{i,m}$ = Simulated daily temperature in particular month;

$T_{i,o}$ = Observed daily temperature in particular month;

T'_i = First step corrected temperature;

T''_i = Second step corrected temperature;

T^* = Corrected temperature.

The mean and standard deviation in the formula is mean and standard deviation for each particular month. To transform simulation from a day in January, the statistical properties of January temperature distribution is used, and so on. This statistical bias adjustment will be done for every single grid in each model simulation, using the statistical properties of the nearest grid of gridded observation (as the resolution of every model simulation and gridded observation differ), for that particular month. Therefore, after the bias adjustment, every single grid in each simulation will be transformed to represent its nearest grid of gridded observation better.

3.3.3 Uncertainty Calculation

In the following chapters, the model ensemble mean from all six simulations will be calculated to quantify the average value of the simulations. Only a small number of model used to calculate the ensemble, therefore, this model ensemble mean is prone to any outlier simulated by the models. However, the model ensemble mean is still the most straightforward method to compare all simulations and the observation at once. Along with the model ensemble mean, an uncertainty value will also be derived, which represent the model spread throughout the calculation period. In this study, the uncertainty value is defined as:

$$UNC = \frac{\sum(T_{max} - T_{min})}{2N}$$

which:

UNC = the uncertainty value;

T_{max} = the maximum value projected by all models;

T_{min} = the minimum value projected by all models;

N = length of the period.

3.4 Extreme Climate Indices

In this study, three extreme climate indices will be calculated based on the principle of the ETCCDI indices calculation. Roughly, ETCCDI indices can be divided into four categories (Alexander et al., 2006). The first category, is the absolute extreme indices, such as the highest maximum temperature or lowest minimum temperature in a year. The second category is the percentile-based-threshold, that is expressed as the number of days that certain (value of) percentile exceeded in a year, or also be called as the annual exceedance. For this type of indices, a baseline period (usually 1961 – 1990) is needed to be defined, to create a distribution of temperature data in which the threshold (percentile) will be derived from. The percentile values that are used in ETCCDI indices are the 90th and 10th percentile, to avoid bias jump as was discussed in Section 2.4. The third category is the number of exceedance of specifically defined threshold, to define certain type of weather event, such as frost days (below 0° C) or summer days (above 25° C). The last category is the duration indices, which is usually used to define a prolonged extreme weather event. The annual occurrence of an event in which a threshold is exceeded for a specific length of time, for instance, a heat wave is defined as more-than-five consecutive days period when the daily maximum temperature is 5° C higher than its average (Frich et al., 2002).

Even though more sophisticated statistical approaches were done for the calculation of ETCCDI indices, such as the bootstrap resampling method to avoid inhomogeneities between the baseline period and the period outside the baseline period (Zhang et al., 2005), going through the same processes with the bias-adjusted simulation is computationally demanding within the timescale of this study. Therefore, simpler indices are defined instead to answer the research questions. To represent extreme hot events, three thresholds will be defined, which consisted of an absolute maximum threshold, a percentile-based-threshold, and one specific threshold that is determined based on impact-related-assessment.

As the impact of extreme hot events on infrastructure in the energy sector is a particular concern in this study, the threshold 30° C is chosen, as being impactful in the energy planting environment, based on the information gathered from an energy company running within the region of study (Figure 3.1). Figure 3.3 illustrates the impact of ambient temperature on the efficiency of the gas turbine to generating power. Two cases of turbine sensitivity are shown, in which red represents the turbine with high sensitivity to ambient temperature and blue represents the low sensitivity case. As shown by Figure 3.3, the efficiency reduced after 0° C for both cases, however, after 30° C, the effect becomes significant, that compressor stops working unexpectedly (British Petroleum, personal communication). The three extreme indices in this study defined in Table 3.2.

Denotation	Definition	Unit
TXx	The maximum value of maximum temperature in a year (annual maximum of daily maximum temperature), or will be called as absolute maximum temperature.	°C
T90	The annual exceedance of percentile 90 th of maximum temperature.	Days
T30C	The annual exceedance of 30° C of maximum temperature.	Days

Table 3.2 Extreme climate indices defined in this study.

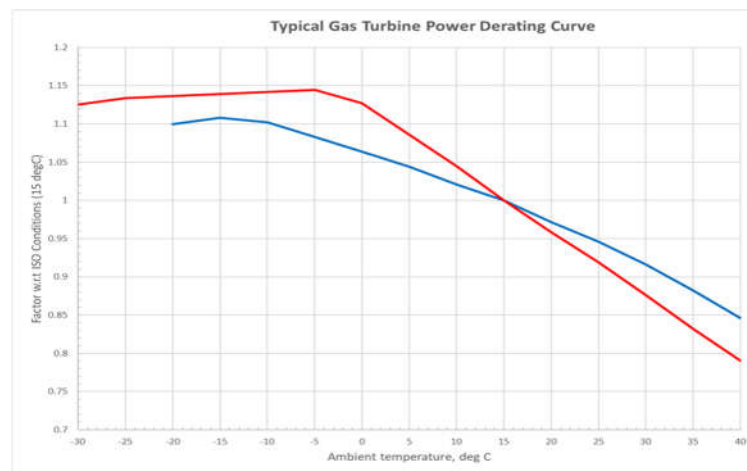


Figure 3.3 Reduced efficiency related with increase in ambient temperature (Source: BP, personal communication). Red line is the curve for turbine with high sensitivity to ambient temperature, while blue line is the low sensitivity case.

The T90 index is designed to measure the frequency of extreme or the number of exceedance over a certain threshold. The threshold is set as the percentile 90th value over a baseline period (defined as 1981 – 2010 in this study), in which this threshold will be calculated for every grid (of the gridded observation, not the model grid). This threshold then will be used to calculate its annual exceedance every year. Therefore, the unit of T90 is the number of days, instead of Celsius. Just like T90 index, the unit for the T30C index is also days, but for the T30C index, the threshold for all grids is the uniform, 30° C. TXx index is aimed to measure the magnitude of the extreme events in a particular year; therefore the unit used is Celsius. The time resolution of those three indices is yearly (annual). Therefore, the trend calculated for those indices will be days/year (for T90 and T30C) and °C/year (for TXx). In parts of this study, the trend of regional average is also calculated to conclude the overall increase of the maximum temperature or extreme indices within that region. In that case, the trend of regional average then implies the trend calculated from the series of regional-averaged-value (for either maximum temperature or extreme indices), instead of the average of trends over a region.

Chapter 4

Drivers of Extreme Hot Events

In this chapter, the possible drivers of temperature pattern and its mechanisms in causing extreme hot events will be discussed. The analysis will be divided into two, which consists of the evaluation for large scale weather pattern and the regional scale weather pattern. Here, the gridded temperature from Berkeley dataset is used to assess the days with highest temperature event (both mean temperature and maximum temperature). This chapter is aimed to provide an overview of the physical processes that lead to extreme hot events, however, this analysis is not aimed as a thorough study.

4.1 Large Scale Drivers of Extreme Hot Events

Large-scale drivers are known to affect the general weather pattern over the Maritime Continent region, such as the Asian-Australian monsoon and tropical SST forcings. The SST variability over both of the surrounding tropical oceans, ENSO and IOD, were also found to affect the temperature pattern over Southeast Asia region and Australia (Chambers and Griffiths, 2008; Tangang et al., 2007). In this first part of the analysis, some statistical approaches are used to evaluate the contribution of El Niño and positive IOD event in causing the extreme hot events.

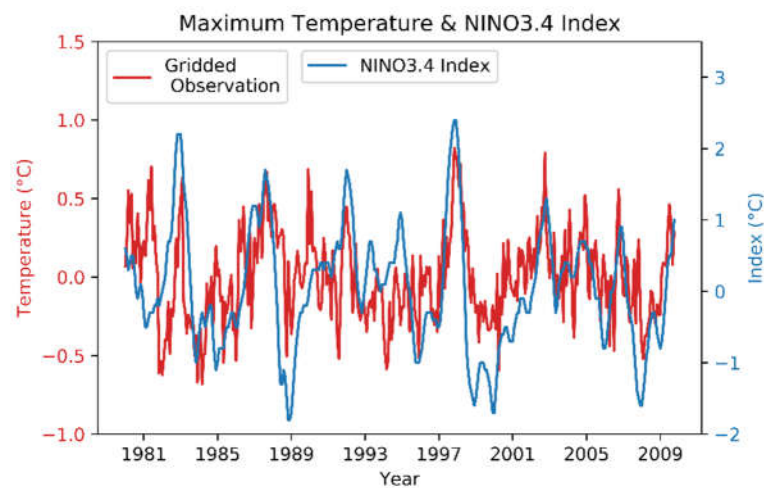


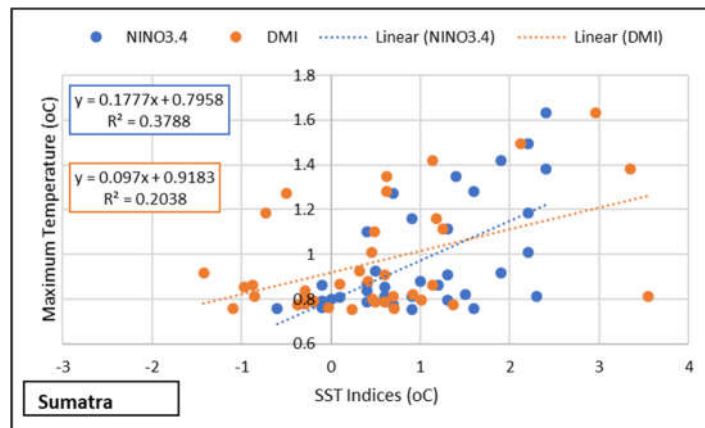
Figure 4.1. Time series of monthly Nino3.4 index (blue) and deseasonalized and detrended regional average of monthly maximum temperature (red). 2 months lag was used, which the El Niño precedes monthly maximum temperature.

In the coupled atmosphere-ocean system, a lagged relationship between monthly maximum SST anomaly and its tropospheric response is expected, and the impact of maximum SST forcing over tropical Pacific to the remote region could take several months lag (Su et al., 2005). 1-month to 5-month lag scenarios are used to examine the relationship between El Niño event and the anomaly of monthly maximum temperature pattern over the Maritime Continent region. Here, monthly maximum temperature means the highest value of maximum temperature in that month, instead of the monthly average of daily maximum temperature. Correlation between both series is calculated to quantify the strength of the association, and 2-month lag is chosen for the analysis as it shows the highest correlation ($r = 0.44$, p -value = 10^{-18}) and gives a good fit between El Niño and monthly maximum temperature event. From Figure 4.1, it can be seen that most of the peak in monthly maximum temperature pattern coincides with a moderate to strong El Niño event, which is marked by the NINO3.4 index being higher than 1. Even though the correlation for the 2-month lag scenario is the highest compared with other scenarios and the relationship is significant, the value still does not indicate a strong relationship between monthly maximum temperature and ENSO event.

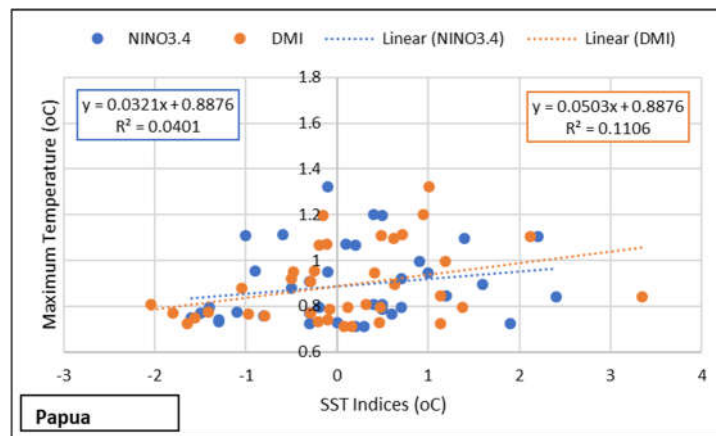
The tropospheric response to each ENSO event is unique due to its varying strength, pattern, and sign. Moreover, the atmospheric response to ENSO event depends on the non-linear relationship between temperature increase and moist convection (Frauen et al., 2014). For an indirect response between SST forcing and monthly maximum temperature events in a remote region, a strong linear relationship cannot be expected. A significant relationship (p -value < 0.05) between IOD and monthly maximum temperature event are only obtained on 4-month and 5-month lag scenario, but the relationship is much weaker than ENSO response ($r < 0.12$). It should be noted that the impact of IOD events is not spatially coherent over the Maritime Continent region in which the regions that are closer to the Indian Ocean such as Sumatra and Borneo are affected more by this variability (Cheong et al., 2018; D'Arrigo and Wilson, 2008) – regional average of temperature profile might not show a useful information about the impact of IOD to temperature in the Maritime Continent region.

To further investigate the role of both modes of SST variability in determining the extreme hot events, 10% of the highest anomaly of monthly maximum temperature events between 1979 – 2010 period (32 year) in each smaller region, the five main islands in the Maritime Continent region (Figure 3.1), are gathered to see the contribution of El Niño and IOD in those events. In that 32-year period, 31% of the highest temperature events coincide with strong and very strong El Niño events (averaged regionally). The NINO3.4 index can explain more than 30% of the variance of the highest maximum temperature in Sumatra, Borneo, and Sulawesi. The highest maximum temperature is less affected by DMI index compared with the NINO3.4 index, but it still contributes to 16 – 29% of the variance of the highest maximum temperature over Sumatra, Borneo, and

Sulawesi. The insignificance of NINO3.4 and DMI index in representing the maximum temperature event in Java and Papua implies that other factors drive the extreme hot events over these regions.



(a)



(b)

Figure 4.2. Scatter plot of NINO3.4 (blue) and DMI (yellow) against 10% highest anomaly of monthly maximum temperature (with 2-month lag), over (a) Sumatra and (b) Papua.

Region	NINO3.4		DMI	
	Trend (°C per °C SST anomaly)	Variance explained (R ²)	Trend (°C per °C SST anomaly)	Variance explained (R ²)
Sumatra	0.18	38%	0.1	20%
Borneo	0.17	38%	0.08	16%
Java	0.03	2%	0.04	9%
Sulawesi	0.12	33%	0.09	29%
Papua	0.03	4%	0.05	11%

Table 4.1. The slope between the anomaly of monthly maximum temperature (10% highest monthly maximum temperature) and the SST anomaly indices in the five main islands, with the corresponding R² value (with 2-month-lag).

When both SST anomalies that has similar response over the Maritime Continent region (for instance, both El Niño and positive IOD events that favour dry condition over the Maritime Continent region) occur simultaneously, more significant impacts are observed, as it amplifies the effect of each SST forcing, causing greater subsidence over this region (Nur'utami and Hidayat, 2016).

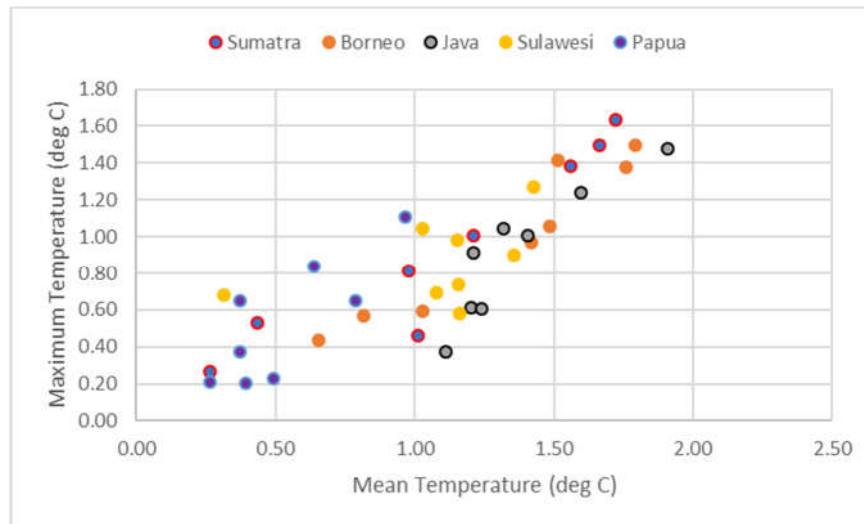


Figure 4.3. The anomaly of monthly mean and maximum temperature in five main islands on the occurrences of simultaneous events of very strong El Niño and positive IOD.

In Figure 4.3, the mean and maximum temperature over each smaller region when strong positive IOD events coincide with very strong El Niño events are plotted. The mean temperature increase over Java region in simultaneous strong IOD and very strong El Niño event is more consistent ($1^{\circ}\text{C} - 2^{\circ}\text{C}$) than Sumatra ($0.3^{\circ}\text{C} - 1.7^{\circ}\text{C}$) and Borneo ($0.6^{\circ}\text{C} - 1.8^{\circ}\text{C}$). This could imply that other smaller scale processes affect extreme hot events over Java. This might be related with the fact that most of Indonesia's biggest cities are located on this island and the UHI (Urban Heat Island) impact is found to be significant in influencing temperature pattern in this island (Siswanto et al., 2016), which implies the consequence of boundary-layer scale processes to extreme hot events. However, the small number of sample available for simultaneous positive IOD and very strong El Niño event means that the conclusion derived above is not statistically robust.

As the main cause of variability over the Maritime Continent region is solar forcing (Li et al., 2017), any weather phenomena that affect the cloudiness over Maritime Continent region, will also affect the temperature variability in this region. In this case, the atmosphere circulation contributes more to the surface temperature profile, instead of the other way around (Trenberth and Shea, 2005). As subsidence happens over the Maritime Continent region, cloudiness is reduced, and this allows more solar radiation to reach the surface. Reduced precipitation also implies a drier soil condition,

which lessens the evaporative cooling effect. ENSO effect on temperature in the Maritime Continent region is not a direct process, as the warming pattern that is associated with El Niño is mainly caused by the subsidence over the Maritime Continent region due to more active convective activity over eastern Pacific (Tangang et al., 2007). The slowly evolving El Niño and its well-known impact for the most part of the world give some level of predictability to the following extreme temperature events (Sillmann et al., 2017). In the future changing climate, the response to these modes of SST variability depends on three aspects, the changes in the SST variability itself, the changes in the way remote region react to a particular SST forcing, and the changes of other large-scale phenomena that might amplify or hinder the impact of the SST variability (Vecchi and Wittenberg, 2010). For an indirect impact of ENSO such as surface temperature variability, the changing response to these SST variabilities will be more chaotic.

4.2 Regional Scale Processes

Whilst El Niño provides an indirect contribution to extreme temperature event; regional scale processes have larger potential to maintain the dry condition that leads to extreme hot events. Case studies are needed as a tool to identify the contribution of other land-atmosphere processes that induce extreme hot events. In this section, other weather patterns that might cause extreme hot events in the tropical region are investigated. As was shown in the previous section, the impact of ENSO and IOD in causing extreme hot events over Java and Papua is lower than other regions.

As was mentioned in Section 1.2, one of the main motivations of this study is to assess the impact of extreme hot events on a power plant site, the location of which is depicted in Figure 3.1. Two case studies from that region are then chosen (red box in Figure 4.2) for illustrative purposes rather than as a detailed investigation. The first one is from 8th to 11th December 2000, as these 4 days were included in the 5 warmest days in 1979 – 2010 period (34.1 – 35° C), in that specific grid (gridded temperature Berkeley). The second case is from 11th – 14th February 2002, as 9th February 2002 is also listed as one of the warmest days over this region (32.3 – 34.1° C). Other local weather parameters were gathered the data from a station inside the grid box (Fakfak observational station). The following are aimed to give an overview of possible drivers in particular extreme cases, as attribution processes need a more thorough numerical experiment.

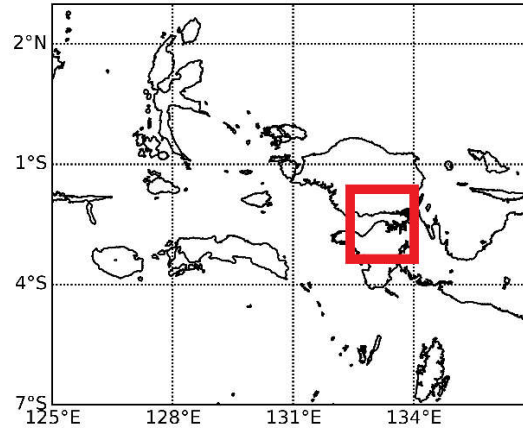


Figure 4.4. The region of interest (red box).

Climatologically, December and February are one of the warmest months for this region as depicted in Figure 4.5. A high-pressure pattern persisted to the north of the region of interest in both cases, causing low wind speed that trapped the heat inside that region. In the first case, the dry condition crept in since the last precipitation recorded, which was on 4 December 2000. As was listed in Table 4.2, below average humidity was recorded, as the average humidity for that month was 78%. Sunshine duration was 100% from 5 December until 9 December, which means more than 8 hours of sunshine exposure in these days. This dry condition affects the soil moisture in since the last precipitation (Figure 4.6). In the second case, the last precipitation recorded was on 8 February 2002, and below average humidity was also recorded, as the average humidity for February in that station is 81% (source: BMKG staff, personal communication).

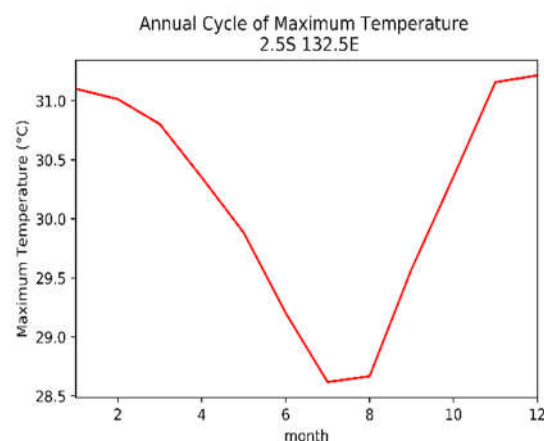


Figure 4.5. Annual cycle of temperature over 2.5°S, 132.5° E (averaged over 2001 – 2010).

	Sunshine Duration (% from 08 – 16 LT)	Humidity (%)	Precipitation (mm/day)
08/02/2002	65	84	3
09/02/2002	100	74	0
10/02/2002	100	72	0
11/02/2002	30	75	0
12/02/2002	35	75	0
13/02/2002	100	74	0
14/02/2002	100	73	0

(a)

	Sunshine Duration (% from 08 – 16 LT)	Humidity (%)	Precipitation (mm/day)
04/12/2000	11	81	4
05/12/2000	100	75	0
06/12/2000	100	75	0
07/12/2000	100	78	0
08/12/2000	100	72	0
09/12/2000	100	76	0
10/12/2000	61	86	0
11/12/2000	54	89	1
12/12/2000	38	82	1

(b)

Table 4.2. Daily weather data from Fakfak observational station (total sunshine duration, average humidity, accumulated rainfall) for (a) case study 1 and (b) case study 2.

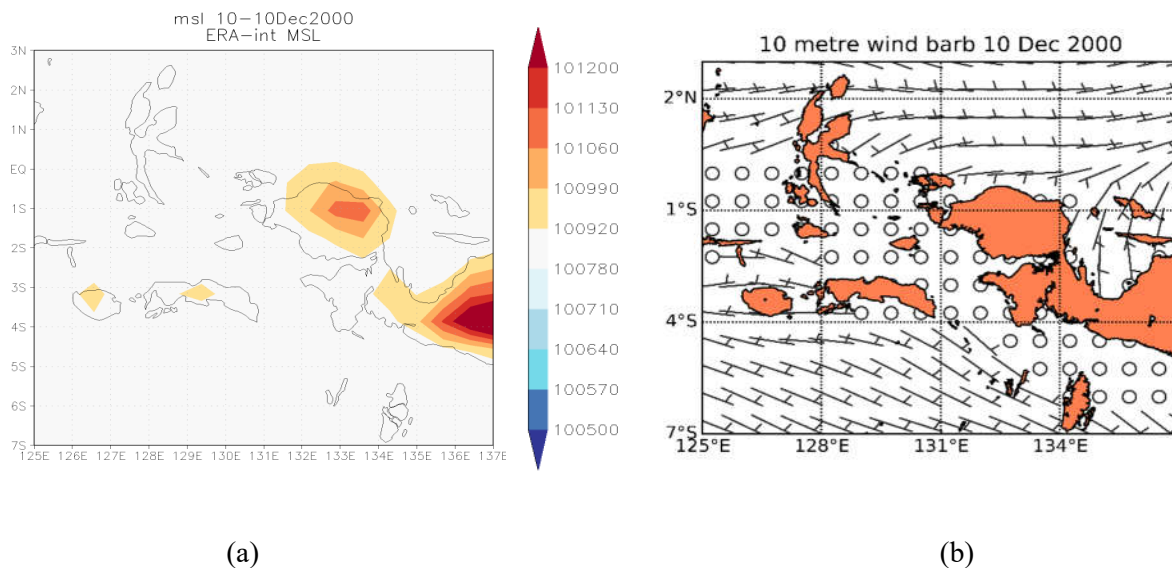


Figure 4.6. (a) Mean sea level pressure (in Pa) (from ERA-Interim dataset) and (b) wind barb (in m/s) (from ERA-Interim dataset) for case study 1 (10 Dec 2000). The same patterns are shown in the second case study.

In both cases, similar patterns of surface level pressure are found, with a high-pressure pattern to the north of the region of interest and further east to the island. This weather pattern was then accompanied with weak wind speed (0 – 1.5 m/s) over the region of interest and the surrounding area. This might imply a reduction of moist advection from the surrounding sea, which impacted on dry condition over land that gradually developed until precipitation occurred. Dry spell also caused a reduction in soil moisture (Figure 4.7), that further amplified the dry condition over land as evaporation reduced. The reduced evaporation that was originally caused by lack of precipitation might act as a feedback, which creates drier condition and inhibits convection. Meanwhile, solar forcing over this region remained strong, and over dry soil, the solar energy is converted more into sensible heat flux, rather than latent heat flux. The only mechanism that can end this loop of feedback is moist advection, that can be achieved as the high-pressure pattern weaken and wind speed increase, and more humidity will be added to the region. Even though the suspected mechanism that caused high temperature for both cases studies are similar, this might not be the case for all region, especially for a vast region with different climatic conditions such as in the Maritime Continent region, as was discussed in section 2.1.

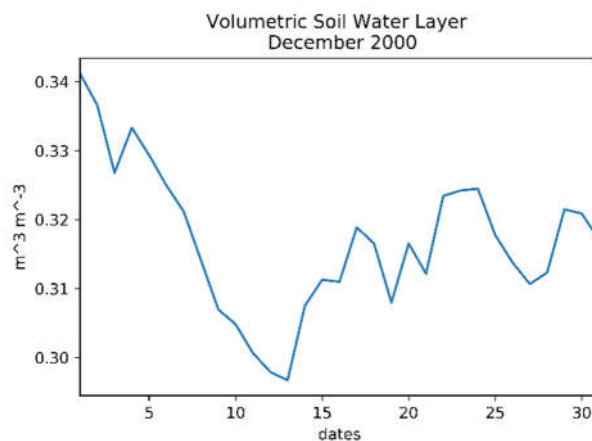


Figure 4.7. Soil water availability (in $m^3 m^{-3}$) for December 2000, indicates the soil moisture (from ERA-Interim dataset).

4.3 Discussion

In the mid-latitude region, extreme temperature events are often associated with large-scale weather pattern such as atmospheric blocking and upper-level circulation pattern (Vavrus et al., 2006; Meehl and Tebaldi, 2004). In tropical Maritime Continent and the surrounding area, extreme hot events are mainly associated with the high solar forcing and precipitation deficit caused by large-scale weather pattern that leads to dry condition (Chambers and Griffiths, 2008; Cheong et al., 2018). The general understanding about physical processes that create the temperature pattern over this region is still less explored compared with the precipitation pattern (Li et al., 2017). Even though large-scale event such as El Niño or IOD gives prior information about the probability of the upcoming extreme temperature event, other smaller scale processes also play a role in determining

the temperature profile. Some mechanisms in the mid-latitude region might also be applied in tropical region, such as how soil moisture affect the evolution of heatwave by creating dry airmass and favoring anticyclonic circulation over the region (Quesada et al., 2012; Zampieri et al., 2009). A deeper understanding of the drivers of extreme hot events in the Maritime Continent region will potentially improve the forecast accuracy and future projection, which have many societal impacts.

The attempt to find the causes of extreme hot events in this chapter is not aimed as a thorough study, but to just gives an overview of the physical processes that affect the extreme hot events in the Maritime Continent region. The large-scale processes described here increase the risk of extreme hot event, however an extreme hot event might happen in a very local region (hot spot) and caused by local factors. The results of this chapter will be used in the following chapters as a physical background of the extreme hot events. In the next chapter, the current profile of extreme hot events will be described, and global climate models will be evaluated based on its ability to represent current extreme.

Chapter 5

Current Extreme and Model Evaluation

In the first section, the gridded observation (Berkeley) will be used to make the spatial distribution of current extreme temperature. In the next section, global climate models will be evaluated using the observed extremes during the observation period (1981 – 2010). As the global climate models are not aimed to predict the exact timing of internal climate variability (Risbey et al., 2014), the model evaluation will be done by comparing trends between the observed extremes and the simulated extremes during the observation period, instead of comparing the exact value.

5.1 Current Extreme

In this section, the current extreme hot event is defined based on the indices that were described in Section 3.4. TXx, or the value of maximum temperature in a year, is the index to show the magnitude of the extreme hot event, while T90 and T30C are aimed to show the frequency of the extreme hot event. In Figure 5.1, the average value of TXx in the observation period (1981 – 2010) for every grid is plotted, to show the spatial distribution of the current extreme.

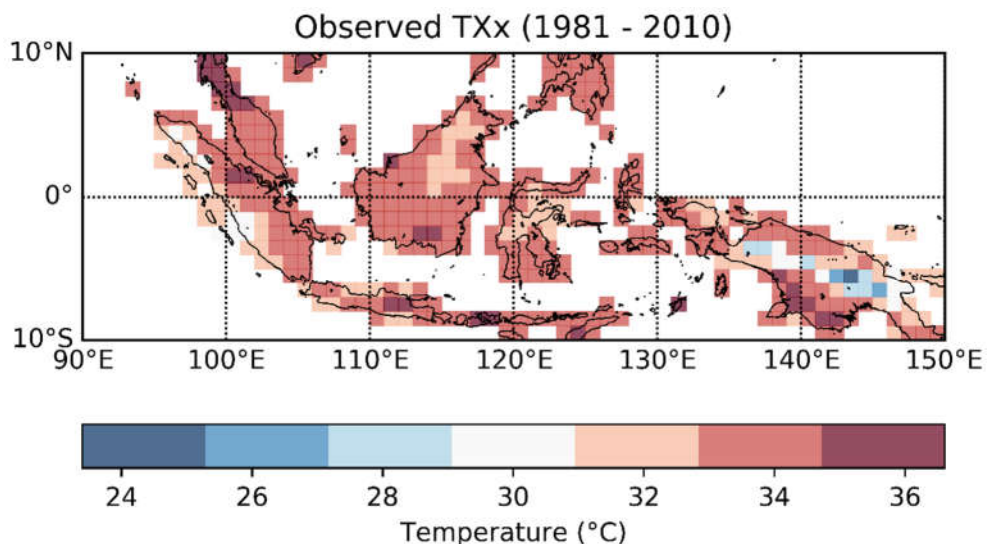


Figure 5.1. Spatial distribution of TXx (averaged over 1981 – 2010 period), from gridded observation.

The TXx is the temperature that only happens once in a year, and this implies the most extreme event in a year. Over the Maritime Continent region, this value varies from 24° C – 36° C. The

coolest part in Maritime Continent region part is over mainland Papua, and the warmest part is further north over Southern Thailand (Songkhla). In Figure 5.1, some relatively cooler TXx can be associated with the topography features, as can be seen in Figure 3.1, such as over west of Sumatra ($30^{\circ}\text{C} - 31^{\circ}\text{C}$), north of Borneo ($30^{\circ}\text{C} - 32^{\circ}\text{C}$), and mainland Papua ($24^{\circ}\text{C} - 28^{\circ}\text{C}$).

As was discussed in Section 3.4, to obtain the T90 index, a certain threshold for every grid was calculated based on the temperature distribution over the baseline period (1981 – 2010), that is plotted in Figure 5.2. The threshold for T90 index indicates a less extreme event compared with TXx and over the Maritime Continent region this value varies from $23^{\circ}\text{C} - 34^{\circ}\text{C}$. The same spatial pattern with TXx in Figure 5.1 is found, which also show the topography influence on temperature profile.

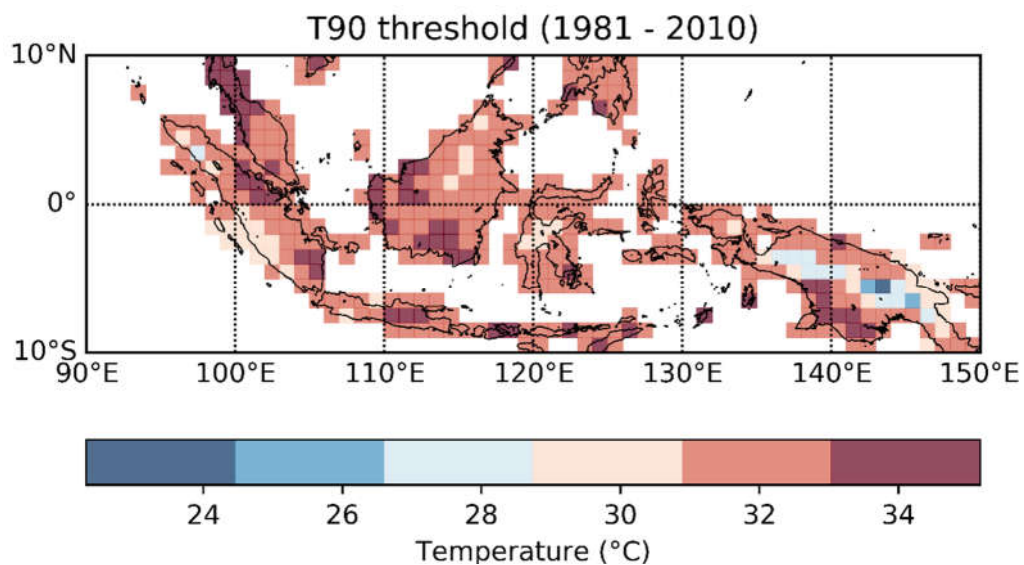


Figure 5.2. Spatial distribution of T90 threshold using 1981 – 2010 baseline, from gridded observation.

5.2 Model Evaluation

Bias adjustment using the variance scaling method (Section 3.3.2) was done to the model simulations before doing any analysis, to transform the mean and variance of the model data closer to the mean and variance of the observation (Teutschbein and Seibert, 2012). In Figure 5.3, the result from bias adjustment is shown, comparing the pdf (probability distribution function) of the daily maximum temperature of HadGEM2-ES and gridded observation from 1981 – 2010 period, averaged over the Maritime Continent region, before (a) and after (b) the bias adjustment. Before the bias adjustment, HadGEM2-ES simulation has lower mean temperature (28.1°C) and smaller standard deviation (0.3°C) compared with the mean (30.3°C) and standard deviation (0.6°C) of the observation. After the bias adjustment, the corrected simulation shows closer mean (30.1°C) and more similar standard deviation (0.56°C) with the observation, however, it should be noted

that the simulation still cannot completely capture the temperature distribution of the observed temperature, which means in general, lower extreme will be simulated.

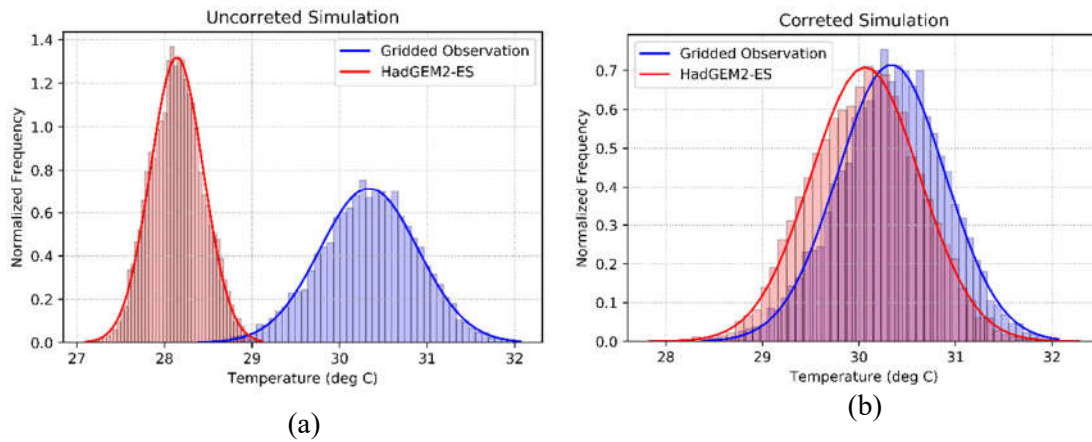


Figure 5.3. Probability density functions (PDFs) of the regional-averaged daily maximum temperature of gridded observation and (a) HadGEM2-ES simulation, (b) corrected HadGEM2-ES simulation, for 1981 – 2010 period.

The model evaluation in this section will be divided into three: the regional average of maximum temperature, the spatial distribution of extreme climate indices, and the regional average of the extreme climate indices. In the next section, some regional-averaged temperature and trend will be calculated, and it implies an averaged value over the Maritime Continent region, over land area. The trend for the maximum temperature is calculated using OLS (ordinary least squares) and the significance is tested using the t-test, in which p -value less than 0.05 is considered as a significant trend.

5.2.1 Regional Average of Maximum Temperature

As the extreme climate indices will be calculated from the maximum temperature, the ability of the models to simulate the maximum temperature will be examined in this section. In Figure 5.4, the regional average (over the Maritime Continent region) of maximum temperature of the gridded observation and climate model simulations are plotted. It should be noted that the maximum temperature here is the average of daily maximum temperature in a particular year, not the TXx index. In this study, to differ between the annual average of maximum temperature and the TXx index, the TXx index will be addressed as absolute maximum instead of annual maximum. In this study, when trend of regional average is stated, it implies the trend calculated from the series of regional-averaged-value (either maximum temperature or the indices) over the Maritime Continent region. In Figure 5.4, the observed maximum temperature lies within the model spread, yet, some significant biases from the models still can be found, such as in 1983 (mean temperature from all models are 0.1 – 0.4° C lower than the observation) and 1992

(mean temperature from all models are 0.1 – 0.8° C lower than the observation). In both cases, the temperature drop in the simulations is suspected to be related with big eruptions in the year before (El Chichón in 1982 and Pinatubo in 1991). A volcanic forcing should be resulted in temporary cooling in the lower troposphere, as the volcanic haze reflect the incoming solar radiation to the lower troposphere. However, in the real observation of temperature, this effect is sometimes offset by other unforced internal variability, such as the volcanic eruption in 1982 that was followed by a strong El Niño in 1982 -1983 (Mélières, 2015). In Table 5.1, all the models show stronger trends than the observation in the observation period, except for MRI-CGCM3. The major cooling simulated by the climate models at the beginning of the observation period might contribute to higher trends relative to the trend of gridded observation.

	Trend (deg C/decade)
Gridded Observation	0.21
HadGEM2-ES	0.23
CNRM-CM5	0.28
GISS-E2-R	0.39
MRI-CGCM3	0.17
BCC-CSM1	0.4
CanESM2	0.36
Model Ensemble	0.31

Table 5.1 Trend of the regional-averaged gridded maximum temperature over the Maritime Continent region (annual average). Non-significant trend is marked by (*).

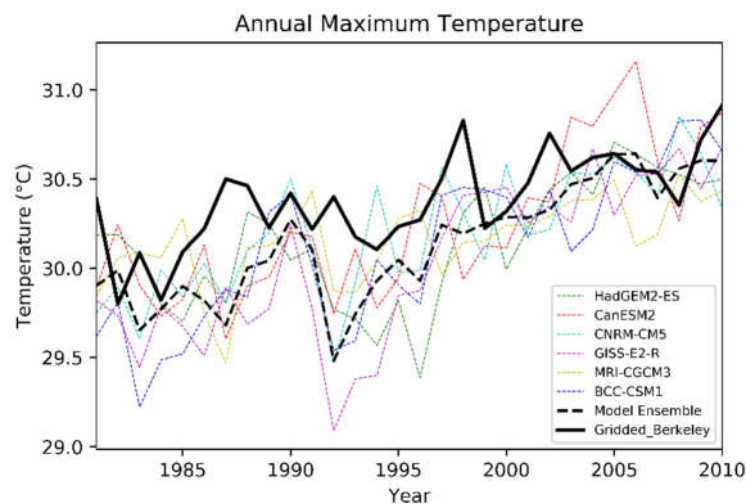


Figure 5.4. Time series of the regional averaged gridded maximum temperature (annual average) over the Maritime Continent region, from 1981 – 2010.

5.2.2 Spatial Distribution of Extreme Climate Indices

The annual average of the observed maximum temperature is generally well simulated by the climate models even though differences in the trends exist. However, as the purpose of this study, the global climate models need to be evaluated on how they can represent the extreme events, rather than the mean value. The trend of extreme climate indices is derived from all the gridded observation and model simulations in the observation period (1981 – 2010), to evaluate model performance in representing the evolution of the magnitude and frequency of extreme events. For T90 and T30C index, trend implies the increase in the annual exceedance (day/year) over the calculation period, meanwhile trend for TXx index implies an increase in absolute maximum temperature ($^{\circ}\text{C}/\text{year}$) over the calculation period.

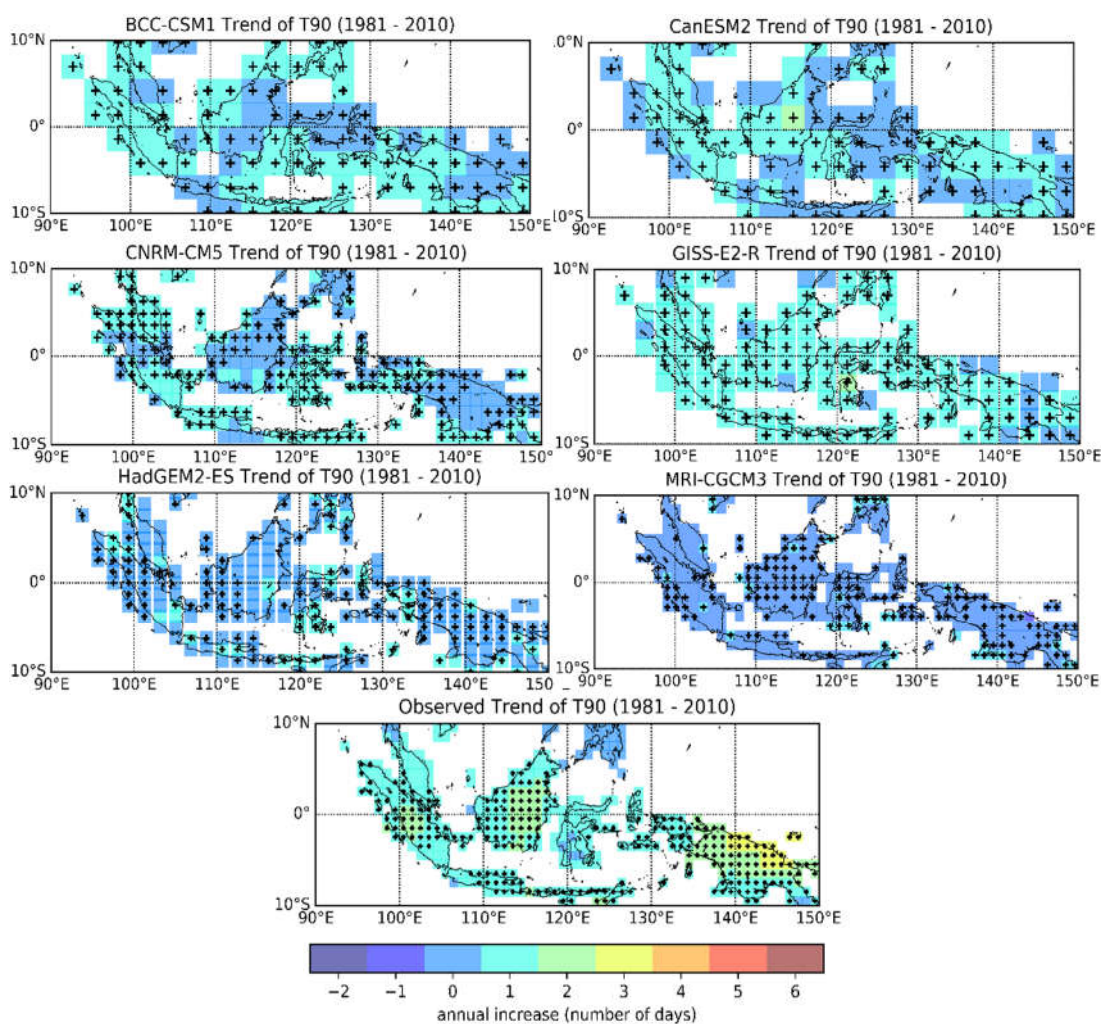


Figure 5.5. The trend of T90 index (day/year) in 1981 – 2010 period. The regions with significant trend at 95% confidence level (p value < 0.05) are marked by the plus sign.

The analysis is done on the native resolution of the models and observation, without re-gridding the resolution. Due to the availability of the data, the observation period used to calculate the

value of the percentile based threshold (T90), is the same as its baseline period, which is 1981 – 2010. The significance and magnitude of the trend of the T90 index for each model and observation are shown in Figure 5.5. In total, 65% of the Maritime Continent region experience a significant increase in the frequency of T90 exceedance. In the map of the observed trend, relatively rapid increases (1 – 3 days/year) (which means 1 – 3 more annual exceedance in every year in 1981 – 2010 period) of the annual exceedance of T90 are found over Papua, Eastern Borneo, and Central Sumatra, and the trends are significant. Generally, models simulate a lower trend than the observed trend of the T90 index and some models even simulate significant negative trend.

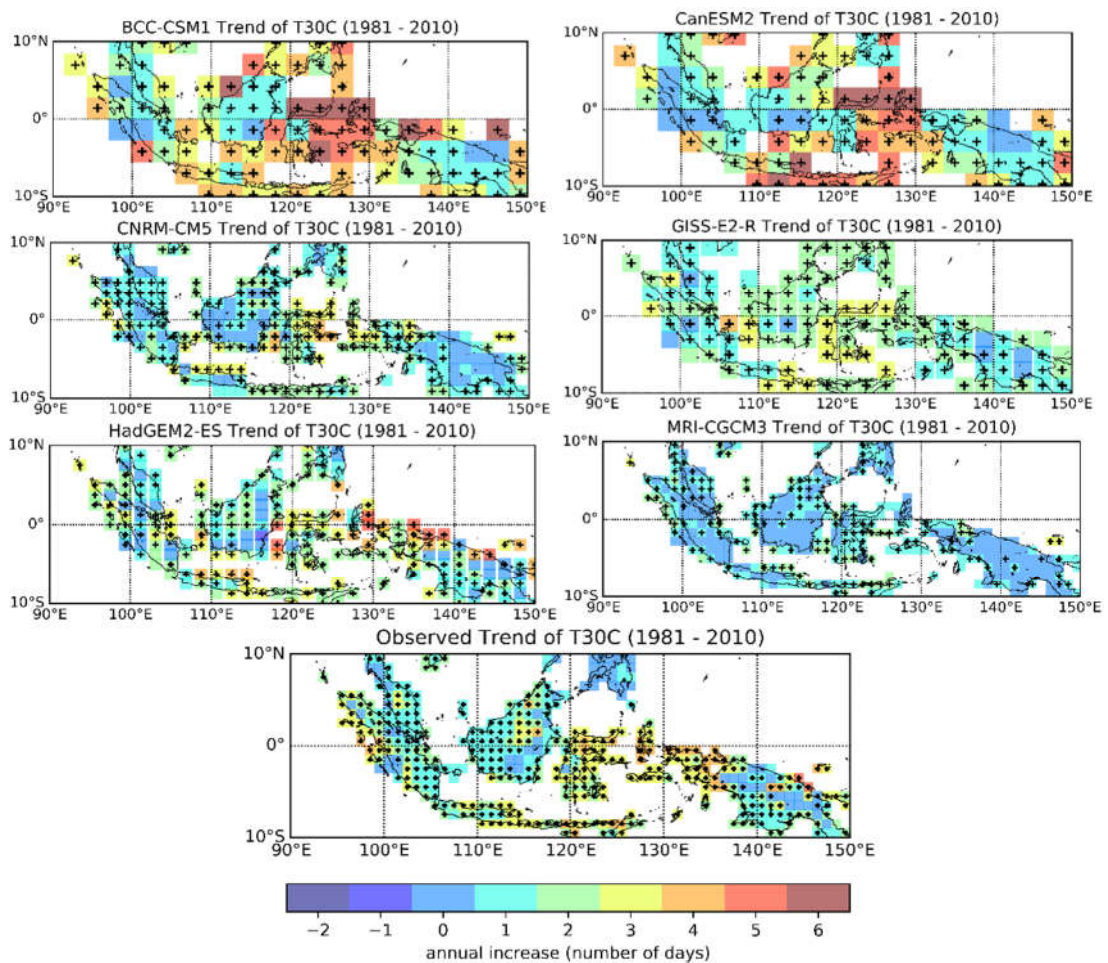


Figure 5.6. The trend of T30C index in 1981 – 2010 period. The regions with significant trend at 95% confidence level (p value < 0.05) are marked by the plus sign.

For the impact-based-threshold index, T30C (Figure 5.6), significant increases in most (81.3%) of the Maritime Continent region are found, except for Philippine, the southern part of Borneo, and parts of Papua. The trends of the T30C over north of Sulawesi and north of Papua are generally higher, by 3 – 5 days/year increase. The significant increase over north of Sulawesi

and north of Papua is also shown by most of the models except MRI-CGCM3, but the magnitude of the trend is stronger than the observed trend, implies more significant warming over this region simulated by the models. For the TXx index (Figure 5.7), only a small portion of the Maritime Continent region (19%) has significant positive trend of TXx index, which is only south of Papua, west of Borneo, and the western part of Malaysia Peninsula, that show significant trend with 0.2° C/decade increase. HadGEM2-ES simulation can simulate the warming pattern over Southern Papua, and the trend over Borneo can generally be simulated by CanESM2, even though the significant increase is simulated to be more extensive.

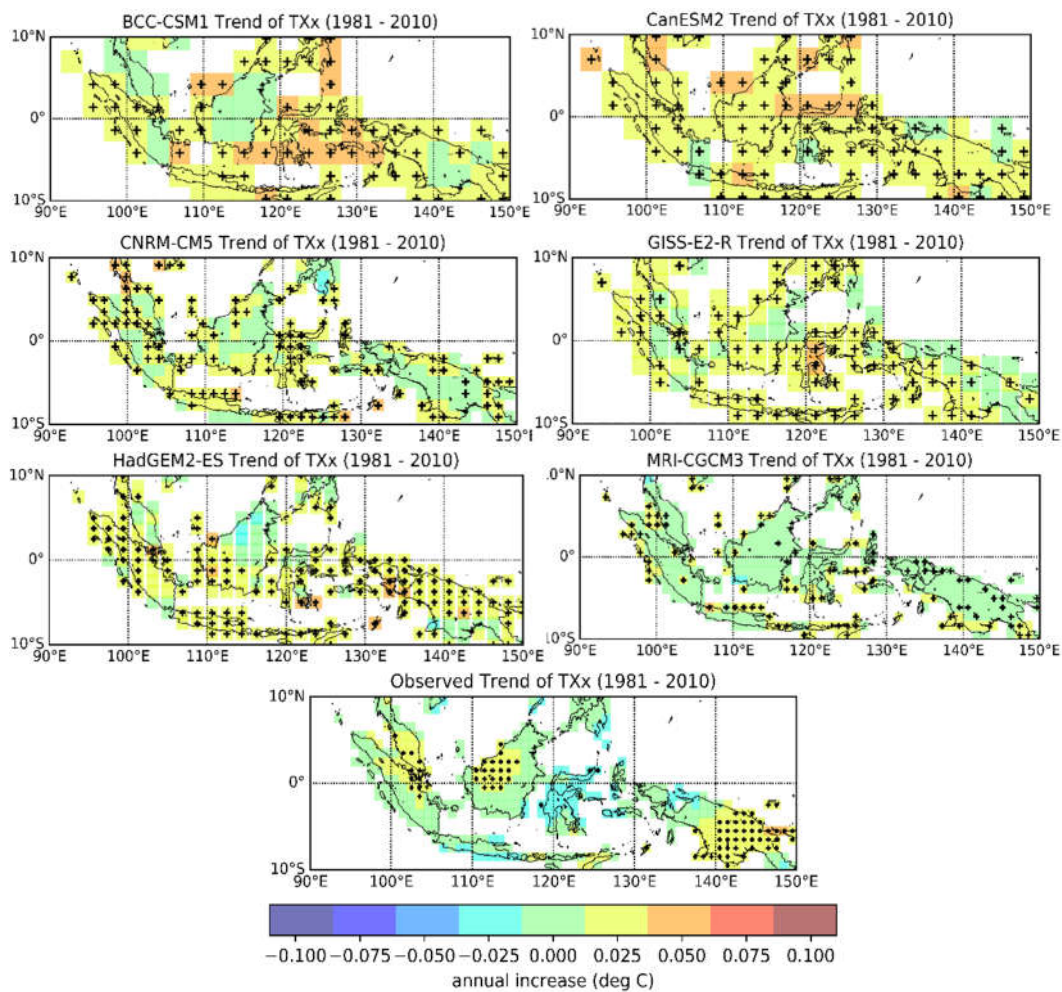


Figure 5.7. The trend of TXx index in 1981 – 2010 period. The regions with significant trend at 95% confidence level (p value < 0.05) are marked by the

In general, some models resemble the spatial pattern of the observed trend to some extent. However, the most pronounced observed warming patterns (such as in the T90 trend, Figure 5.5) are sometimes not well simulated by the models. Most of the Maritime Continent region experience significant increase in the number of exceedance of T90 (65% of the total region) and T30C (81.3% of the total region), but the significant increase in the magnitude of extreme

(TXx) is only found in narrower areas (19% of the total region), implying that the absolute maximum or the most extreme magnitude of high temperature has not changed much since 1981 – 2010 in most regions, but there are more days in a year in which the extreme conditions reached, or more frequent extreme.

5.2.3 Regional Average of Extreme Climate Indices

To quantify the performance of the models in representing the extreme hot event over the Maritime Continent region, the trend of the regional-averaged indices for all simulations and observation is tabulated (Table 5.2) for 1981 – 2010 period. The time series of the regional-averaged indices are plotted (from 1980 – 2017) in Figure 5.8. On a regional scale, the observed trend of TXx index is not significant (p -value > 0.05), and it is suspected that some natural variability affected the absolute maximum value in the observation period. For instance, the El Niño event in 1982 and 1986, which increase the risk of extreme hot events over the Maritime Continent region (Section 4.1), might contribute to the high absolute maximum at the beginning of the observation period, as can be seen in Figure 5.8(c). In Table 5.2, the trend of regional-averaged T30C for all simulations vary from 0.74 – 2.93 days/year, but the model ensemble mean shows comparable value (1.77 days/year) with the observed trend (1.79 days/year). The trend of the regional-averaged T90 shown by all simulations are generally lower than the trend of the regional-averaged observed T90, and the model ensemble shows a much lower trend (0.5 days/year) compared with the observed trend.

	T30C (number of days/year)	T90 (number of days/year)	TXx (deg C/decade)
HadGEM2-ES	1.84	0.34	0.19
CanESM2	2.69	0.6	0.26
CNRM-CM5	1.37	0.5	0.15
GISS-E2-R	1.73	0.7	0.18
MRI-CGCM3	0.74	0.33	0.08
BCC-CSM1	2.93	0.61	0.24
Ensemble	1.77	0.5	0.18
Obervation	1.79	1.21	0.04*

Table 5.2 Trend of regional-averaged extreme indices over the Maritime Continent region (1981 - 2010). Non-significant trend is marked by (*).

From Figure 5.8., the regional-average of the all observed indices is higher than the spread of all models, indicating that even after bias adjustment, model simulations still cannot represent the characteristic of extreme hot events over this region, particularly for the most extreme event such as the TXx index. For the moderate extreme index, such as the one represented by the

percentile-based-threshold index (T90), the bias between the observed index and the simulated index is relatively smaller than other indices (Figure 5.8). However, it should be noted that in this case, the T90 index is calculated over its baseline period (1981 – 2010), therefore, during the 1981 – 2010 period, the multi-annual-mean of annual exceedance of this index will be ± 36 days ($\pm 10\%$ hottest day in a year) by definition. Even though biases exist between the observed and simulated indices, the deviation between the observed extreme and the models in the historical period still can be used for future reference. For instance, in a year (in average, over 1980 – 2017 period), the observed T30C index is higher than the model ensemble by 38.7 days, the observed T90 index is higher than the model ensemble by 25.4 days, and the observed TXx index is higher than the model ensemble by 0.5°C .

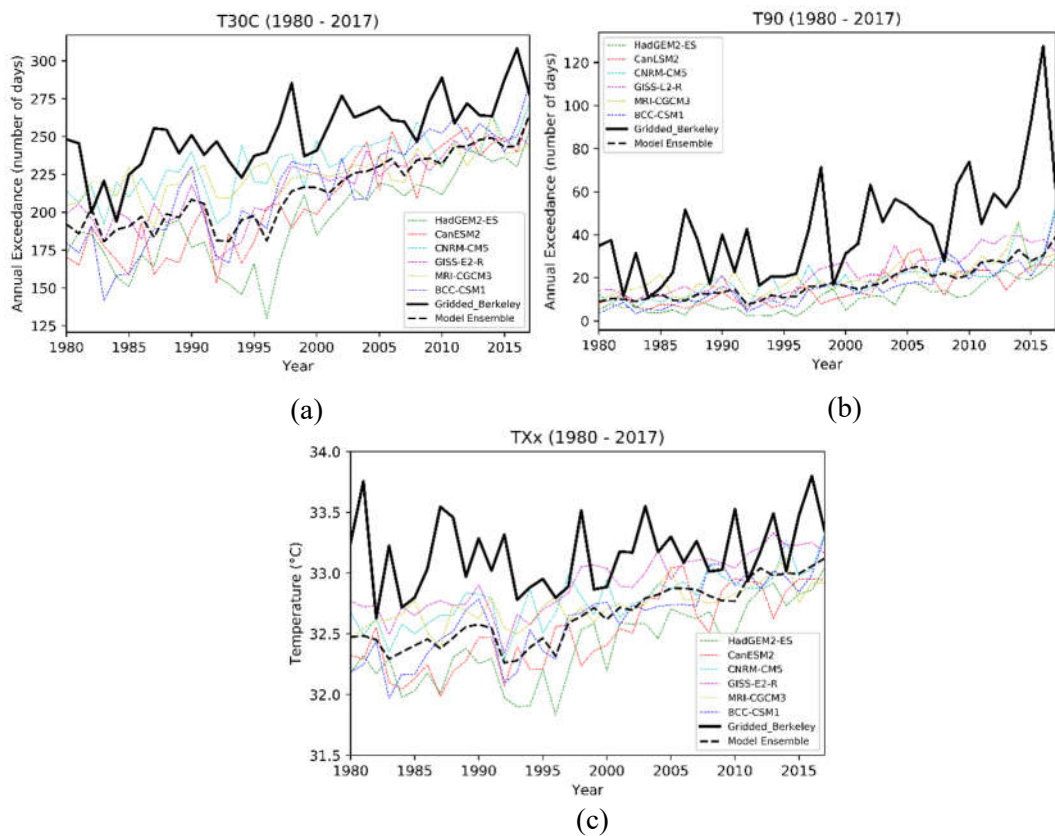


Figure 5.8. The trend of regional-averaged (a) T30C, (b) T90, and (c) TXx indices from all models and observation over the Maritime Continent region (1980 – 2017).

5.3 Discussion

As was discussed in Section 2.2, the Maritime Continent region is characterized by small spatial variability. This can be seen by the pattern of the current extreme in Figure 5.1 and 5.2, using gridded daily maximum temperature. Some warmer grids can be linked with the existence of urban area such as in Songkhla (southern Thailand) (Jongtanom et al., 2011) and Jakarta (western Java)

(Siswanto et al., 2016), but generally, the extreme temperature pattern over the Maritime Continent region largely resemble its topographic feature (Figure 3.1). However, as was discussed in Section 3.1.2, the gridded dataset does not fully represent station extremes. Haylock (2008) quantified the effect of gridding daily temperature for extreme assessment in European land region. For a maximum temperature that only happens once in a ten year period (10-year return level), gridded temperature show a lower value than station by 1.1°C on average. For a region with a small density of observation like the tropical region, the uncertainty in assessing extreme event is suspected to be larger than the region with higher observation density, such as European region (Diffenbaugh et al., 2017).

In this chapter, the performance of global climate models is assessed using the temperature profile from gridded observation. Climate model simulations generally contain unwanted bias for climate change impact assessment (Piani et al., 2010), as can be seen in Figure 5.3. After the bias adjustment, the mean and standard deviation of the model are indeed closer to the observation, but it still not completely captures the observed temperature distribution. There is still some biases that resulted in the observed extreme event becomes higher than the simulated extreme (Figure 5.4, Figure 5.8) and the spatial patterns of the observed trends are not well-simulated by the models (Figure 5.5 – 5.7). This can be caused by the difference in the resolution of the climate models and the gridded observation used for the bias adjustment. In this study, the bias correction was applied to every grid in the models, using the statistical properties of the nearest grid box of the gridded observation. Both grids have different sizes, therefore the data from the coarse resolution of climate models are corrected by data from a smaller region, which might add some level of uncertainty in that bias-adjusted model. Downscaling the climate models before the bias correction will reduce the uncertainty in simulating the temperature profile (Ahmed et al., 2013; Aloysius et al., 2016). In addition, to fully represent the events at the furthest tail of the probability distribution, higher level bias adjustment might be needed, such as quantile mapping, in which the transformation is done based on the position of each value in the probability distribution (Teutschbein and Seibert, 2012).

In this chapter, the changes in frequency and intensity of extreme hot events in the Maritime Continent region are calculated using the gridded temperature from the Berkeley dataset. Three indices are calculated; the percentile based index (T90), impact based index (T30C), and absolute maximum threshold (TXx). The trend of the regional-averaged indices (in 1981 – 2010 period, Table 5.2) are 1.21 days/year for the T90 index, 1.79 days/year for the T30C index, and $0.04^{\circ}\text{C}/\text{decade}$ for TXx index, even though the trend for TXx index is not significant. The indices defined in this study are the simpler version of the ETCCDI indices, as was discussed in section 3.4. Previous studies of extreme temperature events using ETCCDI indices have been done in the regions adjacent to the Maritime Continent region using the station data (e.g., Caesar et al., 2011;

Cheong et al., 2018). Compared to this study, the trend for T90 index (or TX90P in ETCCDI) in those studies were lower; 3.05 % of days in a year per decade (1.1 days/year, from 1972 – 2010) for northern Southeast Asia region (Cheong et al., 2018) and 3.09 % of days in a year per decade (1.1 days/year, from 1970 – 2012) over Indonesia region (Supari et al., 2017). The trend for T90 index calculated in this study is still comparable with those studies (differs by 0.1 days/year), despite the fact that simpler indices are used here. Unlike this study, the regional-average trend of TXx in Cheong et al. (2018) and Supari et al. (2017) are significant, however, the fraction of the station that have significant trend of TXx over Indonesia was relatively small, less than 20% over all Indonesia (19% in this study).

In Figure 5.8(b) it appears that the T90 and T30C peaked significantly on strong El Niño year, but the effect on T90 appears more significant than T30C. The same result was found in Nicholls (2005), in which the number of exceedance of hot days (percentile 99th of daily maximum temperature) increased significantly one year after the El Niño onset in East Asia and West Pacific region, even though the mechanism was not explained. In this study, the regional average of the T90 index in 1998 (the El Niño onset was 1997) is 71 days, and 127 days in 2016. The same effect is not as significant for the absolute maximum TXx, and this might imply that El Niño indeed a contributing factor to increase the TXx index, but various factors other than El Niño can affect the absolute maximum value. After 2000, the similar number of exceedance with the 1998 case happened several times even without strong El Niño event (2002, 63 days; 2010, 73 days), indicates underlying pronounced warming over Maritime Continent region.

As can be seen in Figure 5.8, it is suspected that the natural variability has a dominant effect in the time series of T90 and T30C indices, such as the strong El Niño events in 1997 and 2015. In the historical period, the ENSO simulated by CMIP5 will be out of phase with the historical ENSO and models cannot recreate the timing of year to year climate variability, particularly in the tropical region (Jones et al., 2013) (IPCC, 2014). As the SST in the surrounding region shapes the weather and climate system in the Maritime Continent region, better representation of the SST variability in the climate model is needed to make a more reliable projection of the extreme events (Cheong et al., 2018). To reduce the effect of the natural variability, a better choice of observation period for model evaluation can also be used. In this study, the 30-year period is used, as it is commonly considered sufficient to eliminate the effect of natural variability, hence the fact that this length of the period is the standard for calculating climate normal (WMO, 1989). However, in a rapidly changing climate, this assumption is not always true, as the climate condition within this period cannot always be assumed stationary (Arguez and Vose, 2011). This might as well add more uncertainty to the trend calculated earlier in this chapter.

The annual average of the gridded maximum temperature (Figure 5.4) can generally be simulated by the models used as it lies inside the model spread, even though at the beginning of the observation period, the gridded maximum temperature is slightly higher than the model spread. When the daily maximum temperature is used to calculate extreme indices, some biases arise (Figure 5.8), and the spatial distribution of the trend of extreme climate indices differ by its magnitude and sign (Figure 5.5 – 5.7). However, useful information still can be derived, assuming these biases will remain linear in the future. In the next chapter, the projection of all six climate models will be used to assess the impact of future climate change to extreme hot events in the tropical region, and the results of the model evaluation in this chapter will be used to interpret the projection.

Chapter 6

Future Extreme Hot Events

In this chapter, the projection of the six global climate models for the RCP4.5 (Section 3.3.1) scenario will be used to estimate the changes in extreme hot events in the future. As was discussed in Section 3.3.3, the uncertainty values that are stated in this chapter correspond to the model spread. The conclusion derived from the model evaluation will be used in interpreting the analysis in this chapter.

6.1 Projection of Maximum Temperature

The future projection (from 2017 – 2050) of regional-averaged maximum temperature from all models and the model ensemble mean are plotted in Figure 6.1. Using the model ensemble, the average of maximum temperature over the Maritime Continent region for 2031 – 2050 period (projection period) will be increased by $1.2 \pm 0.4^\circ \text{C}$, compared with 1986 – 2005 period (current period). The trend of annual-average maximum temperature (Table 6.1) over the Maritime Continent region (from 2021 – 2050) shown by the models are approximately $0.3^\circ \text{C/decade}$, except for the HadGEM2-ES simulation which shows the highest increase of the annual average of maximum temperature ($0.43^\circ \text{C/decade}$). The trend of the model ensemble calculated in this period is $0.35^\circ \text{C/decade}$. However, as the trend of the model ensemble in the observation period (Section 5.2.1) is larger ($0.31^\circ \text{C/decade}$) than the observed trend ($0.21^\circ \text{C/decade}$), this might imply that the real trend for 2021 – 2050 period will also be smaller than calculated in this section.

	Trend (deg C/decade)
HadGEM2-ES	0.43
CNRM-CM5	0.3
GISS-E2-R	0.3
MRI-CGCM3	0.3
BCC-CSM1	0.34
CanESM2	0.34
Model Ensemble	0.35

Table 6.1 Trend of the regional average of maximum temperature projection (2021 – 2050) over the Maritime Continent region.

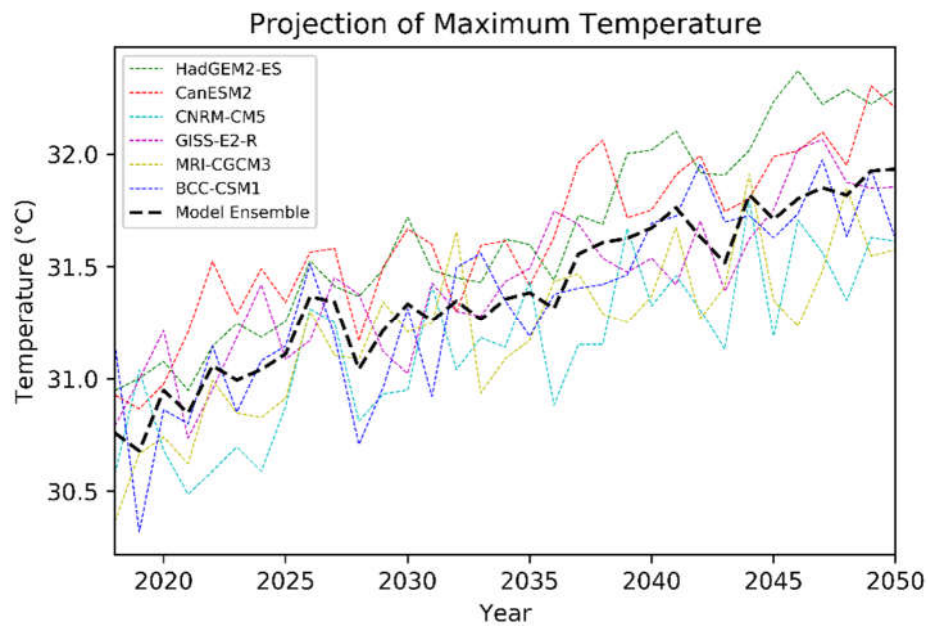


Figure 6.1 Time series of regional average of maximum temperature projection (annual average) over the Maritime Continent region (2018 – 2050).

6.2 Spatial Distribution of Extreme Climate Indices

In Figure 5.5, all models show a relatively smaller trend of the T90 index (0 – 1 days/year), compared with the observed T90 (1 – 3 days/year). In Figure 6.3, slower pattern of warming is still shown by CNRM-CM5, GISS-E2-R, and MRI-CGCM3 (0 – 2 days/year) but other models show a larger trend of warming (1 – 7 days/year), especially HadGEM2-ES, indicating the differences in the performance of climate models in representing the extreme indices. In Figure 6.3, generally, more extensive pattern of significant warming (compared with Figure 5.5) is projected over the Maritime Continent region, which implies a more spatially coherent pattern of warming in the future period.

In Figure 6.4, the spatial pattern of the T30C index in the 2021 – 2050 period is plotted. Unlike the trend of the T90 index, the trend of T30C index projected by the models is generally lower than in Figure 5.6 (observation period), especially for BCC-CSM1 and CanESM2 simulations. Some regions even have a negative trend of the T30C index during the 2021 - 2050 period in the BCC-CSM1 and CanESM2 simulations, even though the regional trend is positive (Table 6.2). It is worth noting that in some simulations, particularly the ones with higher resolution (CNRM-CM5, HadGEM2-ES and MRI-CGCM3), the extensive highland area over the Maritime Continent region (as depicted in Figure 3.1) such as west coast of Sumatra, northern Borneo, and north and mainland Papua, are projected to have relatively higher trend (1 – 5 days/year) of T30C compared with its surrounding region. The high number of exceedance for T30C over the Maritime Continent region

in general (± 252 days, regional-averaged over the Maritime Continent region, averaged over 1980 – 2017

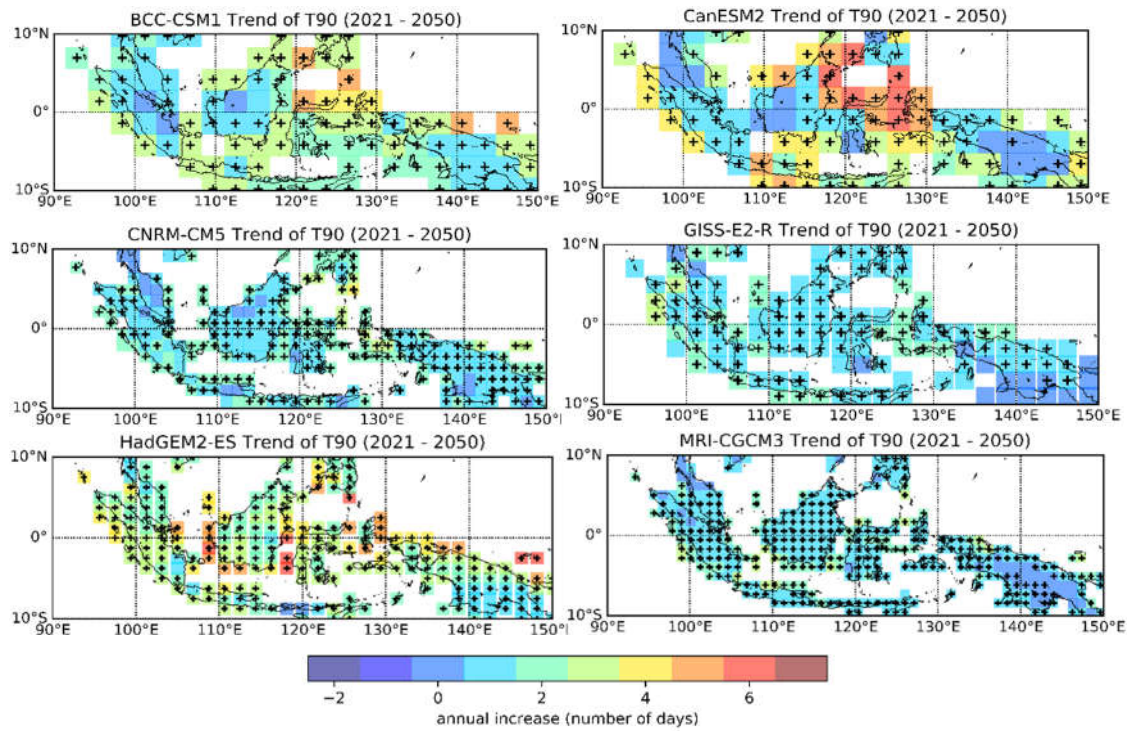


Figure 6.3 The trend of T90 index in 2021 – 2050 period. The regions with significant trend at 95% confidence level (p value < 0.05) are marked by the plus sign.

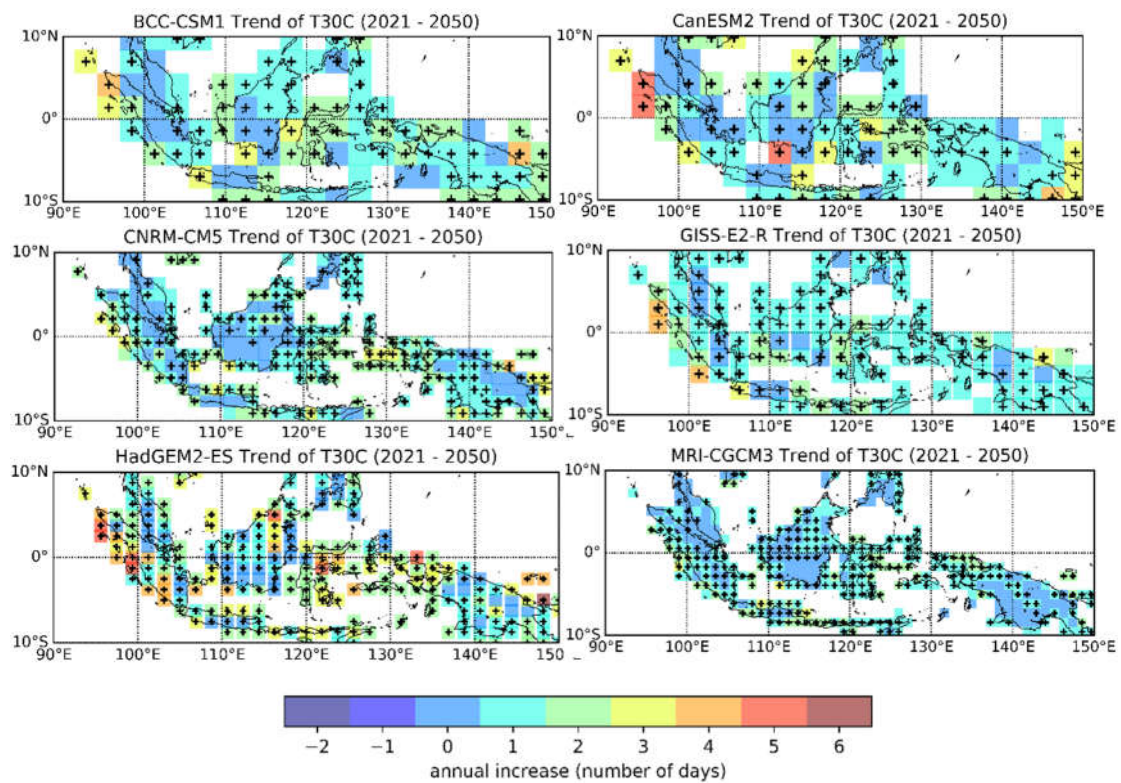


Figure 6.4 The trend of T30C index in 2021 – 2050 period. The regions with significant trend at 95% confidence level (p value < 0.05) are marked by the plus sign.

period) implies that most of the days in a year has higher than 30° C maximum temperature already and there are not much days in a year left to be exceeded. Therefore, the rate of exceedance for T30C is expected to be lower than the higher percentile index (T90, for instance). However, high terrain area has relatively much lower temperature compared with lowland (Figure 5.1). Therefore, the number of exceedance of T30C in the observation period is lower than the regional average here. This allows a higher rate of exceedance for the T30C index over high terrain area in the future period.

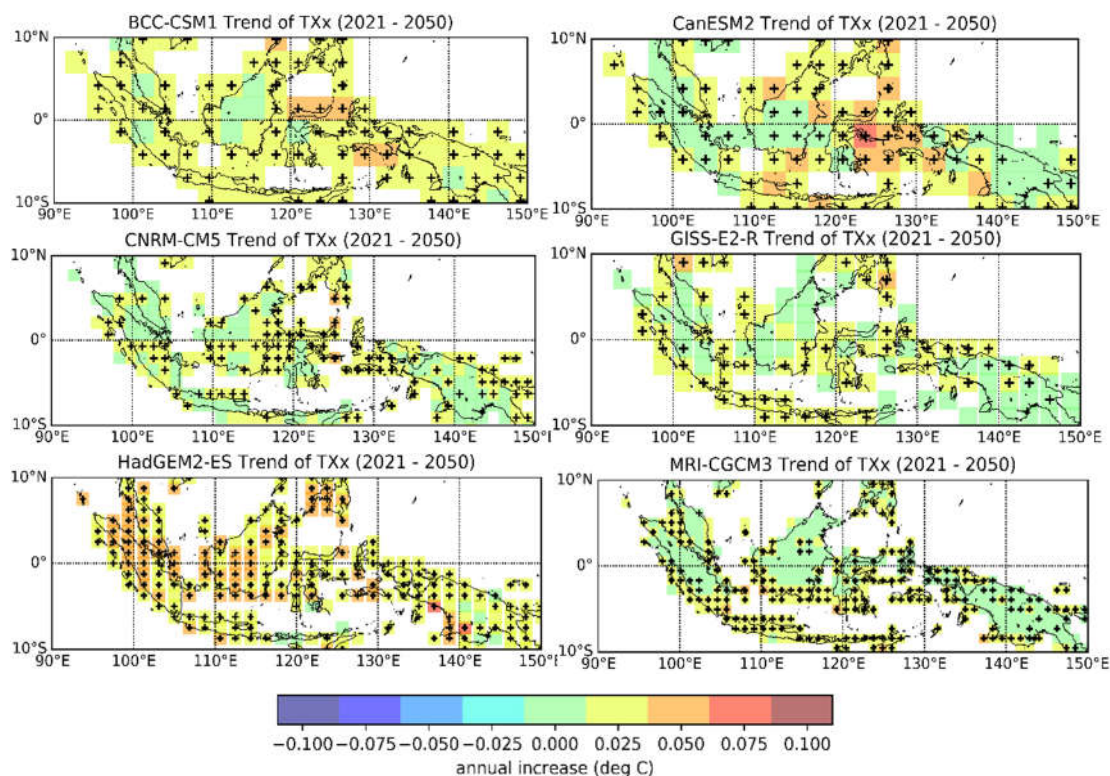


Figure 6.5 The trend of TXx index in 2021 – 2050 period. The regions with significant trend at 95% confidence level (p value < 0.05) are marked by the plus sign.

In Figure 6.5, compared with Figure 5.7 (observation period), a more extensive pattern of significant warming is simulated by HadGEM2-ES, although the same conclusion cannot be said for other models. In general, the trend for simulated TXx index in the future period is approximately similar to the observation period, 0 – 0.5° C/decade. The warming pattern shown by simulations in Figures 6.3 – 6.5 vary by its magnitude and significance, and it shows model uncertainty in projecting the extreme climate event. However, it still provides some useful information when a rough estimate of warming over a certain location is needed, as will be shown later in Section 6.4.

6.3 Regional Average of Extreme Climate Indices

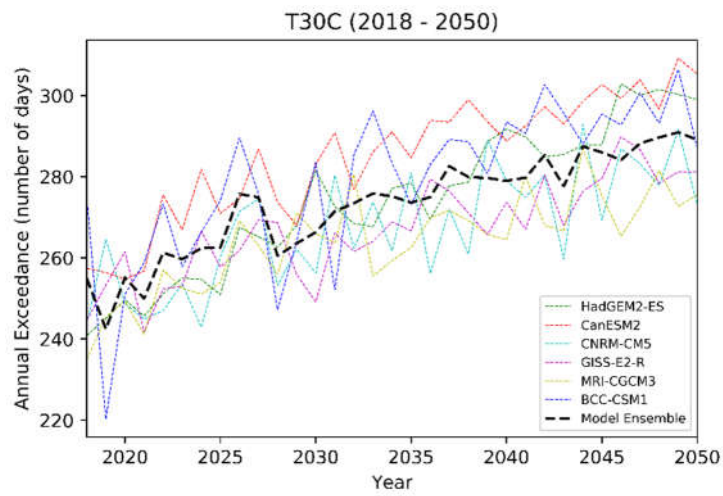
The trend of regional-averaged indices in 2021 – 2050 period is tabulated in Table 6.2, to quantify the rate of change of the extreme hot event in the future period (2021 – 2050) over Maritime Continent region. Compared with the observation period (Table 5.2) the trend of regional-averaged T30C index simulated in the future period by most simulations are generally lower, except for HadGEM2-ES and MRI-CGCM3 simulations. In the observation period, the trend shown by the model ensemble of the regional-averaged T30C index is 1.77 days/year; in the future period, the trend shown by the model ensemble is only 1.2 days/year, which means a slower increase of regional-averaged of T30C exceedance. As was discussed in Section 6.2, the annual exceedance of T30C is already high enough in the observation period (± 252 days, regional-averaged over the Maritime Continent region, averaged over 1980 – 2017 period), that means not many days in a year left to be exceeded, therefore, the slower increase of T30C exceedance does not necessarily imply a slower rate of warming in the future.

For the T90 index, all models simulate a higher trend of the regional-averaged T90 index in the future period, compared with the simulated trend in the observation period (Table 5.2), which implies a faster rate of warming is expected in the future period. It should also be noted that the observed trend of the T90 index in Table 5.2 (1.21 days/year) is higher than all simulations (0.3 – 0.7 days/year) in the observation period, which implies the models underestimate the rate of warming shown by observed T90 index. It is possible that this higher-than-simulated trend will be continued in the future period, which means, the real trend will be higher than the trend of the model ensemble in the future period, or higher than 1.8 days/year.

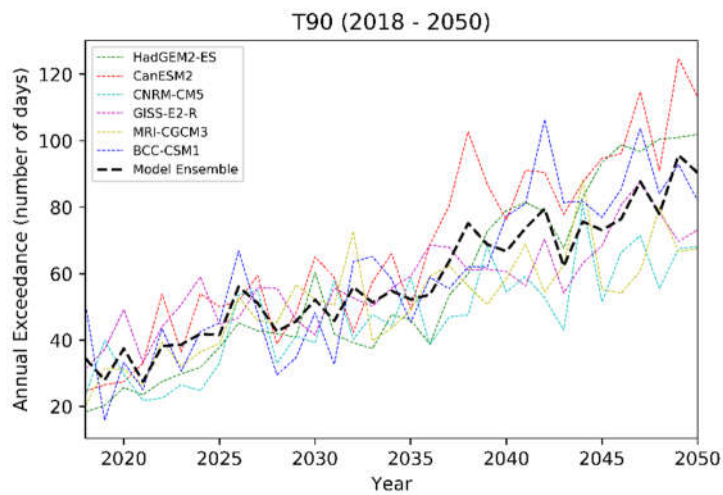
For the TXx index, the trend of the regional-averaged index over Maritime Continent projected by model simulations (0.14 – 0.32° C/decade) is comparable with the trend simulated in the observation period (0.08 – 0.26 °C/decade). However, in the observation period, the observed trend for TXx index is much lower than the simulations; therefore, the trend shown by the TXx in future might not as high as the trend projected by the model simulations. The fact that the trend of the regional-averaged TXx is not even significant, implies a challenge in interpreting any result regarding the TXx index.

	T30C (number of days/year)	T90 (number of days/year)	TXx (deg C/decade)
HadGEM2-ES	1.8	2.6	0.32
CanESM2	1.45	2.6	0.24
CNRM-CM5	1.09	1.3	0.15
GISS-E2-R	1.04	1.16	0.14
MRI-CGCM3	0.97	1.28	0.17
BCC-CSM1	1.45	2.06	0.23
Ensemble	1.2	1.8	0.18

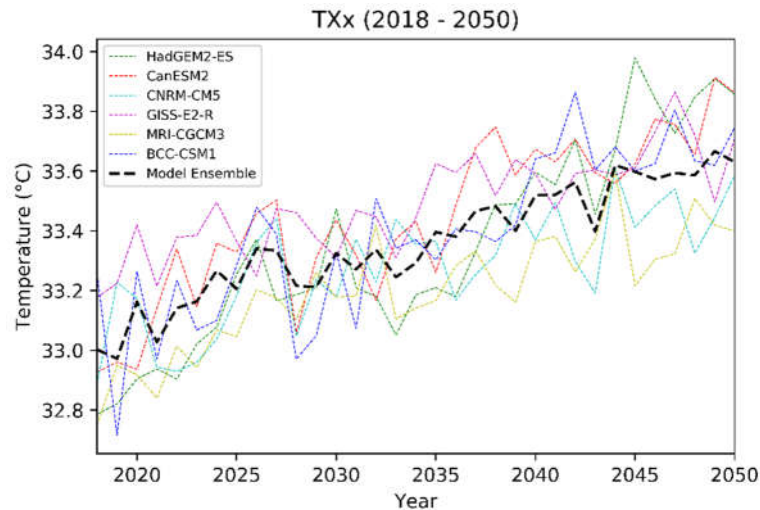
Table 6.2. Trend of regional average of extreme indices (2021 - 2050) over the Maritime Continent region. Non-significant trend is marked by (*).



(a)



(b)



(c)

Figure 6.6. The regional average of future (2018 – 2050) projection of (a) T30C, (b) T90, and (c) TXx over the Maritime Continent region.

Using the model ensemble, compared with the 1986 – 2005 period (current period), the annual exceedance of T30C in 2031 – 2050 (projection period) will be increased by 41 ± 20 days, the annual exceedance of T90 in 2031 – 2050 period will be increased by 55 ± 7 days, and the TXx will be increased by $0.9 \pm 0.2^\circ$ C. However, from Section 5.2, it should be noted that there are biases between the time series of the regional average of the simulated indices (represented by the model ensemble) and the observed indices. For instance, as in the observation period the observed T30C is generally higher than the model ensemble by 38.7 days (every year), this implies much fewer days in a year to be exceeded, and the trend in the future period will be lower than the trend of model ensemble (lower than 1.2 days/year), as annual trend can be affected by high annual of exceedance (as was discussed in Section 6.2). Therefore, the increase of T30C index is suspected to be lower than 41 ± 20 days in the 2031 – 2050 period), although further investigation of physical mechanisms is required to establish this.

For the T90 index, the observed trend of the regional-averaged T90 index in the observation period (1.21 days/year) is higher than the simulated (0.5 days/year for model ensemble). If this higher-than-simulated trend persists in the future, the real increase of T90 in 2031 - 2050 period compared with current period (1986 – 2005) might be larger than was suggested earlier (55 ± 7 days).

For the TXx index, as in the observation period the trend of the regional-averaged TXx is much lower than the simulated trends, it might implies that the real trend of the TXx index will be lower in the future period, however, as was discussed earlier, the trend of regional-averaged TXx is not significant; it cannot be used in deriving any conclusion regarding the trend of TXx. Further

analysis of the causes of the discrepancy between observed and simulated trends (e.g., internal variability, uncertainty in forcing and their influence on atmospheric circulation) is required to interpret the reliability of future projections.

6.4 Projection of Extreme Hot Event in Energy Planting Site

As was mentioned in Section 1.2, one of the main motivations of this study is to assess the impact of future climate change on infrastructure in the energy sector, specifically gas turbine power which works inefficiently above 30°C as was discussed in Section 3.4 and which is represented by the impact-based-threshold index, T30C. The location of the site is in the northern Papua, as was shown in Figure 3.1. In Figure 6.4, most of the models are showing a significant increase of trend of T30C over this region, except for the CanESM2, with 1 – 3 days/year increase projected in 2021 – 2050.

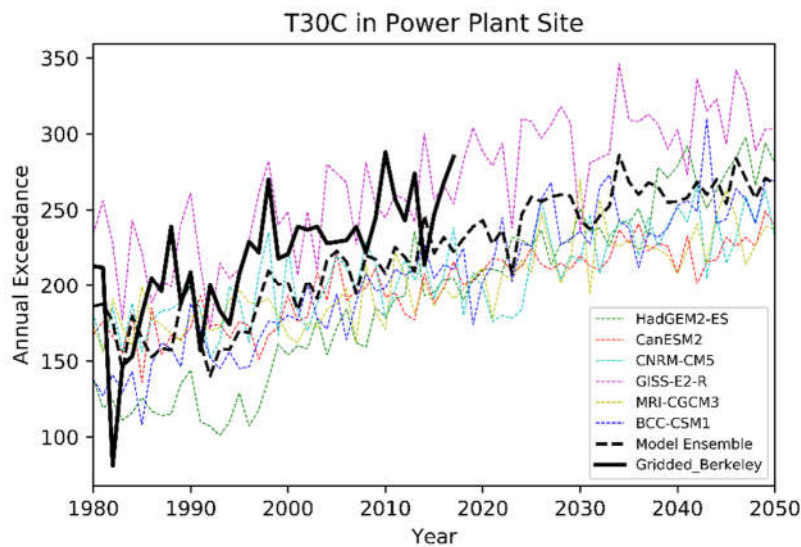


Figure 6.7. The time series (1980 – 2050) of T30C over the region of interest (North Papua).

In Figure 6.7, the T30C index from all simulations in 1980 – 2050 period in the grid of the power plant site (Figure 3.1) is plotted. A wide model spread of the annual exceedance of T30C implies a wide uncertainty of the projection. Using 1986 – 2005 as the baseline period, the annual exceedance of T30C in 2031 – 2050 will be increased by 81 ± 40 days. Here, the high uncertainty value is caused by the high simulation by GISS-E2-R within this particular grid. In the observation period, the model ensemble mean is lower than the observation by 25.9 days. Combined with the projected change, this implies a high annual exceedance of T30C, to the point that it represents a mean condition instead of extreme event. This condition is unfavourable in such gas turbine power plant environment, as the density of the air decrease with increasing ambient temperature, and the

compressor has to exert more power to increase the air pressure, which means reduced efficiency (Farouk et al., 2013).

6.5 Discussion

In interpreting the extreme climate indices to the real-life application, the ideas behind those indices have to be understood. The percentile based index (T90) and impact based index (T30C) depict the changes in the frequency of extreme events, while TXx depicts the magnitude of the extreme hot event. The less extreme events (such as T90) are generally more statistically robust as more data are available for the analysis, yet has less impact to society (Zhang et al., 2011). In this study, TXx is the most extreme index compared with other indices, as it only occurs once in every year. Even though the model spread in the TXx projection indicates a comparable warming rate for all models ($\pm 0.3^\circ \text{C}/\text{decade}$), as was discussed in Chapter 5, the trend of the simulated TXx index is much faster than the observed TXx in the observation period. On the other hand, the absolute maximum temperature (TXx) shown by the observation is always higher than the model simulation (Figure 5.8.c). Therefore, the largest uncertainty actually exists while interpreting the changes in the TXx index in this study.

While the future magnitude of extreme (TXx) calculated in this study is not conclusive, the frequency of the extreme event is projected to increase at a faster rate than in the observation period, which is >1.8 days/year in 2021 – 2050 period (for T90). Even though the projected trend of T30C is smaller (model ensemble, 1.2 days/year) than the observational period (1.77 days/year), the fact that its number of exceedance already implies mean condition instead of an extreme event, this renders it no longer representative as the threshold for extreme event.

The more pronounce increase in the frequency of extreme hot event over the Maritime Continent region is also shown in a global study by Sillmann et al. (2013b), which the trend of the warm days (or TX90P, the annual exceedance of percentile 90th index) is projected to be the highest in the tropical region, particularly Southeast Asia, even though the trend of the absolute maximum (TXx) is comparable with other regions on earth in 2081 – 2100 period. This is mainly attributed to the small temperature variability over the tropical region, that is a small increase in the mean value means a much higher annual exceedance of high-temperature-threshold. In another global study, Russo et al. (2014) derive a metric to calculate heatwave severity by using both the magnitude (temperature increase) and frequency of heat wave (HWMI, Heat wave magnitude index). Even though the temperature increase over Indonesia region is not as high as midlatitude region, Indonesia is listed as one of the region with the highest HWMI due to its high projected frequency of high extreme exceedance. The same pattern of warming is also shown in the surrounding region. In Australia, it is projected that in 2081 – 2100 the frequency of heat wave event in northern

Australia will be increased by 25 days in every summer (Cowan et al., 2014). However, the magnitude of these heat wave event is projected to increase less significantly in northern Australia (0.4 – 0.8 °C) compared with the southern region (1.6 - 3°C), yet the frequency and duration of the heatwave are more substantial in northern Australia compared with southern Australia. The small increase of the absolute maximum temperature over time can be associated with the upper limit of temperature in the humid tropical region. The much warmer condition in the humid region can increase instability that leads to convection. The precipitation resulted from this mechanism will cool the air near the surface (Sherwood and Huber, 2010).

Chapter 7

Conclusions

7.1 Conclusion

This study examined the impact of future climate change on extreme hot events in the Maritime Continent region. Climate model simulations are used to depict the changes in frequency and magnitude of extreme hot events in the future. Gridded observations are used to represent the current extreme temperature over the Maritime Continent region, using extreme climate indices. The performance of climate model simulations is examined based on its ability to represent the current extreme climate indices. The drivers of extreme hot events are also briefly discussed. In general, the results show that there will be a significant increase in the frequency of extreme event in the future period, even though the magnitude change of extreme hot event in this study is not conclusive. For humid, tropical region, the changes of the frequency of extreme heat are projected to be more pronounced compared with the changes of the magnitude (Sherwood and Huber, 2010; Cowan et al., 2014).

Large-scale weather pattern can induce prolonged dry and hot condition over the Maritime Continent region. The impact of two main modes of SST variability over the adjacent oceans, ENSO and IOD, on maximum temperature over the Maritime Continent region, are examined. Both El Niño and positive IOD event affect the maximum temperature by causing subsidence over the Maritime Continent region that reduces cloud cover and precipitation (Tangang et al., 2007). This reduced cloud cover allows more sunshine to reach the surface and favours dry condition over land, which in turn reduces evaporative cooling and results in increased sensible heat (Trenberth and Shea, 2005). Both modes of variability can be associated with extreme hot events especially over Sumatra, Borneo, and Sulawesi, which El Niño can explain 30% of the variability of extreme hot event over these regions and IOD can explain 16 – 29% of the variability. Smaller scale processes such as persisting high mean sea level pressure that associated with the stable condition over an area might lead to the dryer and warmer condition, however, more detailed study is needed to advance understanding of the physical mechanisms further.

Three indices are used to represent the frequency and magnitude of extreme hot events over Maritime Continent region, which are the percentile-based-threshold index (T90), impact-based-

threshold index (T30C), and absolute value index (TXx). Over 1981 – 2010 period, there is a significant increase of the annual frequency of extreme event, and this is consistent with the extreme climate studies in the surrounding region (Cheong et al., 2018; Supari et al., 2017). However, the increase of the absolute maximum temperature is not as significant, which is suspected to be related to the existence of high natural variability at the beginning of the observation period. Climate model simulations are evaluated based on their representativeness to the current extreme event. Even after bias-adjusted, there are still some biases and differences between the models simulation and gridded observation. It is suspected that this is caused by the imperfect statistical bias adjustment, the difference in the resolution of model simulations and gridded observation, and the model inability to predict natural variability in the correct phase. Nevertheless, the conclusions derived from the model evaluation can be used to interpret the model projection in the future period.

The projection of maximum temperature and extreme climate indices were conducted using the mid-level scenario (RCP4.5). The daily maximum temperature in 2031 – 2050 period is projected to increase by $1.2 \pm 0.4^\circ \text{C}$ compared with the 1986 – 2005 period. The annual exceedance of T30C will be increased by 41 ± 20 days in 2031 – 2050 compared with 1986 – 2005 period, yet, given the high annual exceedance of T30C, this index is not an ideal metric to assess the changes of extreme hot event over Maritime Continent region. In the 2031 – 2050 period, the annual exceedance of extreme hot event, the highest 10th percentile of daily maximum temperature in the baseline period (1981 – 2010) (T90), is projected to increase by 55 ± 7 days compared with the 1986 – 2005 period. However, it is argued that this value may be an underestimation, based upon the comparisons with the trend simulated in the observation period. As the ecosystem and infrastructure over the Maritime Continent region are accustomed to the small variability of temperature, such an increase in the near future will likely lead to significant societal and ecological impact (Harrington et al., 2016; Mora et al., 2013b; Rinawati et al., 2013).

7.2 Limitations and Further Work

An attempt to quantify the changes in extreme hot events in the future changing climate has been conducted, yet, there are various limitations that need to be addressed to make a more reliable assessment. The datasets that are used in this study (gridded observation and individual model simulations) have their own uncertainty and without careful treatment, much larger uncertainty will appear in the result. The fact that the gridded observation cannot completely capture the extreme at station level (Figure 3.2), add more uncertainty to the results presented here. Gridded observation tend to be less extreme and has lower variance compared with station observation, as it shows averaged value over a wider area (Gaitan, 2016). In addition, the Maritime Continent region has less observational station compared with other region, such as Europe. The more station used in the gridding process, the more gridded observation represent the temperature profile over the region

(Diffenbaugh et al., 2017). To examine and project the extreme climate events over a region, gridding the extreme indices calculated from the station data to a regular grid can be a better method, as it provides a better representation of station extreme, instead of calculating the extreme indices using gridded maximum temperature (Donat et al., 2013; Haylock et al., 2008), as gridded indices still inherit the variability of the individual station. Gridded indices are also more consistent with model simulations compared with point-based observation, which allows more straightforward evaluation of the climate models.

For the model simulation, only six models are used here to represent the current extreme and future extreme hot event. The small number of models used here implies that a single outlier in the models could significantly affect the model ensemble pattern and the analysis. In addition, even after bias-adjusted, the models still cannot completely represent the observed temperature distribution (Figure 5.3). A higher number of simulation used does not necessarily imply a more robust projection, however, the impact of outliers, such as in Figure 6.7, can be minimalized. Downscaling the simulation to higher resolution can also improve the bias adjustment performance. As was discussed in Section 5.3, downscaling all model simulations before bias adjustment to the same resolution with the observation is beneficial in terms of allowing more straightforward evaluation between models and lower resolution projection is more impact relevant compared with the coarse one (Ahmed et al., 2013; Aloysius et al., 2016). A similar resolution between the observation and climate models will also make a quantitative evaluation of the spatial distribution of trend possible, unlike the qualitative assessment in this study.

Even though the spatial variability of temperature over the Maritime Continent region is low, a focused analysis on a certain region is necessary, as each region still have differences in their temperature profile. For instance, the annual cycle over the southern part and northern part of Maritime Continent region are differ, given the difference in land-sea distribution and seasonal cycle of the solar forcing (Li et al., 2017). A region-focused assessment will also be more relevant to impact analysis, as the regional average of a wide area might eliminate the small-scale details that contain certain characteristic of every region. In this study, an impact-based-threshold is defined based on the necessity in a certain sector. Over Maritime Continent region, various user-defined threshold can be applied to any important aspect in this region, such as in agriculture (Rivington et al., 2013) and disaster risk assessment (Wu et al., 2013).

REFERENCES

- A. Muller, R., R. Rohde, R. Jacobsen, E. Muller, and C. Wickham, 2013: A New Estimate of the Average Earth Surface Land Temperature Spanning 1753 to 2011. *Geoinformatics & Geostatistics*, **01**, doi:10.4172/2327-4581.1000101.
- Ahmed, K.F., Wang, G., Silander, J., Wilson, A.M., Allen, J.M., Horton, R., Anyah, R., 2013: Statistical downscaling and bias correction of climate model outputs for climate change impact assessment in the U.S. northeast. *Global and Planetary Change* **100**, 320–332, <https://doi.org/10.1016/j.gloplacha.2012.11.003>.
- Aloysius, N., J. Sheffield, J. Sainers, H. Li, and E. Wood, 2016: Evaluation of historical and future simulations of precipitation and temperature in central Africa from CMIP5 climate models. *J. Geophys. Res.: Atmos.*, **121**, 130-152, doi:10.1002/2015jd023656.
- Aldrian, E., 2008: *Meteorologi Laut Indonesia*. Jakarta, 252 pp.
- Aldrian, E., and R. Dwi Susanto, 2003: Identification of three dominant rainfall regions within Indonesia and their relationship to sea surface temperature. *Int. J. Climatol.*, **23**, 1435-1452, doi:10.1002/joc.950.
- Alexander, L.V., and Coauthors., 2006: Global observed changes in daily climate extremes of temperature and precipitation. *J. Geophys. Res.*, **111**, <https://doi.org/10.1029/2005JD006290>.
- Añel J, Fernández-González M, Labandeira X, López-Otero Xde la Torre L, 2017: Impact of Cold Waves and Heat Waves on the Energy Production Sector. *Atmosphere*, **8**, 209, DOI: 10.3390/atmos8110209.
- As-syakur A, Adnyana I, Mahendra M, Arthana I, Merit I, Kasa I, Ekayanti N, Nuarsa ISunarta I. 2014. Observation of spatial patterns on the rainfall response to ENSO and IOD over Indonesia using TRMM Multisatellite Precipitation Analysis (TMPA). *Int. J. Climatol.*, **34**, 3825-3839, DOI: 10.1002/joc.3939.

- Caesar, J., and Coauthors, 2011: Changes in temperature and precipitation extremes over the Indo-Pacific region from 1971 to 2005. *Int. J. Climatol.*, **31**, 791–801, <https://doi.org/10.1002/joc.2118>.
- Case, M., Ardiansyah, F. and Spector, E., 2007: Climate Change in Indonesia. Implications for Humans and Nature (Gland, Switzerland: World Wide Fund for Nature (WWF)).
- Chambers, L.E., Griffiths, G.M., 2008: The changing nature of temperature extremes in Australia and New Zealand. *Aust. Meteorol. Mag.*, **23**.
- Cheong, W.K., and Coauthors, 2018: Observed and modelled temperature and precipitation extremes over Southeast Asia from 1972 to 2010. *Int. J. Climatol.*, <https://doi.org/10.1002/joc.5479>.
- Choi, G., and Coauthors, 2009: Changes in means and extreme events of temperature and precipitation in the Asia-Pacific Network region, 1955-2007. *Int. J. Climatol.*, **29**, 1906–1925, <https://doi.org/10.1002/joc.1979>
- Christensen, J.H., Boberg, F., Christensen, O.B., Lucas-Picher, P., 2008: On the need for bias correction of regional climate change projections of temperature and precipitation. *Geophys. Res. Lett.*, **35**, <https://doi.org/10.1029/2008GL035694>.
- Collins, W.J., and Coauthors, 2008: *Evaluation of HadGEM2 model*, 47 pp.
- Cowan, T. et al. 2014: More frequent, longer, and hotter heat waves for Australia in the twenty-first century. *J. Climate*, **27**, 5851–5871.
- D'Arrigo, R., Wilson, R., 2008: El Niño and Indian Ocean influences on Indonesian drought: implications for forecasting rainfall and crop productivity. *Int. J. Climatol.*, **28**, 611–616, <https://doi.org/10.1002/joc.1654>.
- Dee, Dick, Fasullo, John, Shea, Dennis, Walsh, John & National Center for Atmospheric Research Staff (Eds). Last modified 12 Dec 2016. "The Climate Data Guide: Atmospheric Reanalysis: Overview & Comparison Tables." Retrieved from <https://climatedataguide.ucar.edu/climate-data/atmospheric-reanalysis-overview-comparison-tables>.

- Diffenbaugh, N.S., and Coauthors, 2017: Quantifying the influence of global warming on unprecedented extreme climate events. *Proc. Natl. Acad. Sci.*, **114**, 4881–4886, <https://doi.org/10.1073/pnas.1618082114>.
- Donat, M.G., and Coauthors, 2013: Updated analyses of temperature and precipitation extreme indices since the beginning of the twentieth century: The HadEX2 dataset: HADEX2-global gridded climate extremes. *J. Geophys. Res.: Atmos.*, **118**, 2098–2118, <https://doi.org/10.1002/jgrd.50150>.
- Dosio, A., Mentaschi, L., Fischer, E.M., Wyser, K., 2018: Extreme heat waves under 1.5 °C and 2 °C global warming. *Environ. Res. Lett.*, **13**, <https://doi.org/10.1088/1748-9326/aab827>.
- ENES, 2018: CMIP5 Models and Grid Resolution — vERC. [Portal.enes.org](http://portal.enes.org), <https://portal.enes.org/data/enes-model-data/cmip5/resolution> (Accessed August 1, 2018).
- Farouk, N., Sheng, L., Hayat, Q., 2013: Effect of Ambient Temperature on the Performance of Gas Turbines Power Plant.
- Frauen, C., Dommenges, D., Tyrrell, N., Rezný, M., 2014: Analysis of the Nonlinearity of El Niño–Southern Oscillation Teleconnections. *J. Climate*, **27**, 20.
- Folland, C.K., and Coauthors, 1999: Workshop on indices and indicators for climate extremes, Asheville, NC, USA, 3–6 June 1997 Breakout Group C: temperature indices for climate extremes. *Climatic Change*, **42(1)**, 31–43 pp.
- Frich, P., L. V. Alexander, P. Della-Marta, B. Gleason, M. Haylock, A. M. G. Klein Tank, and T. Peterson, 2002: Observed coherent changes in climatic extremes during the second half of the twentieth century. *Clim. Res.*, **19**, 193–212.
- Gasparri, A., and Coauthors, 2017: Projections of temperature-related excess mortality under climate change scenarios. *The Lancet Planetary Health*, **1**, e360–e367, [https://doi.org/10.1016/S2542-5196\(17\)30156-0](https://doi.org/10.1016/S2542-5196(17)30156-0).
- Gervais, M., Tremblay, L.B., Gyakum, J.R., Atallah, E., 2014: Representing Extremes in a Daily Gridded Precipitation Analysis over the United States: Impacts of Station Density, Resolution, and Gridding Methods. *J. Climate*, **27**, 5201–5218. <https://doi.org/10.1175/JCLI-D-13-00319.1>.

- Griffiths, G.M., and Coauthors, 2005: Change in mean temperature as a predictor of extreme temperature change in the Asia-Pacific region. *Int. J. Climatol.*, **25**, 1301–1330, <https://doi.org/10.1002/joc.1194>.
- Halpert, M.S. and Ropelewski, C.F., 1992: Surface temperature patterns associated with the Southern Oscillation. *J. Climate*, **5(6)**, 577-593.
- Harger J. 1995: Air temperature variations and ENSO effects in Indonesia, the Philippines and El Salvador: ENSO patterns and changes from 1866–1993. *Atmos. Environ*, **29**, 1919–1942.
- Harrington, L.J., Frame, D.J., Fischer, E.M., Hawkins, E., Joshi, M., Jones, C.D., 2016: Poorest countries experience earlier anthropogenic emergence of daily temperature extremes. *Environ. Res. Lett.*, **11**, <https://doi.org/10.1088/1748-9326/11/5/055007>.
- Hawkins, E., Sutton, R., 2009: The Potential to Narrow Uncertainty in Regional Climate Predictions. *Bull. Amer. Meteor. Soc.*, **90**, 1095–1108, <https://doi.org/10.1175/2009BAMS2607.1>.
- Haylock, M.R., Hofstra, N., Klein Tank, A.M.G., Klok, E.J., Jones, P.D., New, M., 2008: A European daily high-resolution gridded data set of surface temperature and precipitation for 1950–2006. *J. Geophys. Res.*, **113**. <https://doi.org/10.1029/2008JD010201>.
- Hendon, H.H., 2003: Indonesian Rainfall Variability: Impacts of ENSO and Local Air–Sea Interaction. *J. Climate*, **16**, 16.
- Hidayat, R., 2016: Modulation of Indonesian Rainfall Variability by the Madden-Julian Oscillation. *Procedia Environ. Sci.*, **33**, 167–177, <https://doi.org/10.1016/j.proenv.2016.03.067>.
- Hofstra, N., Haylock, M., New, M., Jones, P.D., 2009: Testing E-OBS European high-resolution gridded data set of daily precipitation and surface temperature. *J. Geophys. Res.*, 114, <https://doi.org/10.1029/2009JD011799>.
- Im, E.-S., Kang, S., Eltahir, E.A.B., 2018: Projections of rising heat stress over the western Maritime Continent from dynamically downscaled climate simulations. *Global and Planetary Change* **165**, 160–172, <https://doi.org/10.1016/j.gloplacha.2018.02.014>.

- Imada, Y., Shiogama, H., Takahashi, C., Watanabe, M., Mori, M., Kamae, Y., Maeda, S., 2018: Climate Change Increased the Likelihood of the 2016 Heat Extremes in Asia. *Bull. Amer. Meteor. Soc.*, **99**, 97–101, <https://doi.org/10.1175/BAMS-D-17-0109.1>,
- IPCC, 2014: *Climate Change 2014: Synthesis Report. Contribution of Working Groups I, II and III to the Fifth Assessment Report of the Intergovernmental Panel on Climate Change [Core Writing Team, R.K. Pachauri and L.A. Meyer (eds.)]*. IPCC, Geneva, Switzerland, 151 pp.
- Jones, G.S., Stott, P.A., Christidis, N., 2013: Attribution of observed historical near-surface temperature variations to anthropogenic and natural causes using CMIP5 simulations: Attribution of temperatures with CMIP5. *J. Geophys. Res.: Atmos.*, **118**, 4001–4024. <https://doi.org/10.1002/jgrd.50239>.
- Jongtanom, Y., Kositanont, C., Baulert, S., 2011: Temporal Variations of Urban Heat Island Intensity in Three Major Cities, Thailand. *Modern Applied Science*, **5**. <https://doi.org/10.5539/mas.v5n5p105>.
- Kakaras, E., 2006: Inlet Air Cooling Methods for Gas Turbine Based Power Plant. *ASME*, **128**, 312–317.
- Kharin, V.V., Zwiers, F.W., Zhang, X., Hegerl, G.C., 2007: Changes in Temperature and Precipitation Extremes in the IPCC Ensemble of Global Coupled Model Simulations. *J. Climate*, **20**, 1419–1444. <https://doi.org/10.1175/JCLI4066.1>.
- Kiktev, D., Sexton, D.M.H., Alexander, L., Folland, C.K., 2003: Comparison of Modeled and Observed Trends in Indices of Daily Climate Extremes. *J. Climate*, **16**, 3560–3571. [https://doi.org/10.1175/1520-0442\(2003\)016<3560:COMAOT>2.0.CO;2](https://doi.org/10.1175/1520-0442(2003)016<3560:COMAOT>2.0.CO;2).
- Klein Tank, A.M.G., and Coauthors, 2002: Daily dataset of 20th-century surface air temperature and precipitation series for the European Climate Assessment: European temperature and precipitation series. *Int. J. Climatol.*, **22**, 1441–1453. <https://doi.org/10.1002/joc.773>.
- Li, Y., Yang, S., Deng, Y., Hu, X., Cai, M., 2017: A process-level attribution of the annual cycle of surface temperature over the Maritime Continent. *Clim. Dyn.*, <https://doi.org/10.1007/s00382-017-4043-9>.

- Manton, M.J., and Coauthors., 2001: Trends in extreme daily rainfall and temperature in Southeast Asia and the South Pacific: 1961-1998. *Int. J. Climatol.*, **21**, 269–284. <https://doi.org/10.1002/joc.610>.
- Marjuki, van der Schrier, G., Klein Tank, A.M.G., van den Besselaar, E.J.M., Nurhayati, Swarinoto, Y.S., 2016: Observed Trends and Variability in Climate Indices Relevant for Crop Yields in Southeast Asia. *J. Clim.*, **29**, 2651–2669, <https://doi.org/10.1175/JCLI-D-14-00574.1>.
- Mélieres, M-A and Maréchal, C. 2015: *Climate Change: Past, Present and Future*. Chichester: Wiley-Blackwell, Science, Technology and Business.
- Mora, C., Frazier, and Coauthors, 2013: The projected timing of climate departure from recent variability. *Nature*, **502**, 183–187, <https://doi.org/10.1038/nature12540>.
- Nicholls, N., 2005: The El Niño–Southern Oscillation and daily temperature extremes in east Asia and the west Pacific. *Geophys. Res. Lett.*, **32**, <https://doi.org/10.1029/2005GL022621>.
- Nur'utami, M.N., Hidayat, R., 2016. Influences of IOD and ENSO to Indonesian Rainfall Variability: Role of Atmosphere-ocean Interaction in the Indo-pacific Sector. *Procedia Environ. Sci.*, **33**, 196–203, <https://doi.org/10.1016/j.proenv.2016.03.070>.
- Otto, F.E.L., van Oldenborgh, G.J., Eden, J., Stott, P.A., Karoly, D.J., Allen, M.R., 2016: The attribution question. *Nat. Clim. Change*, **6**, 813–816, <https://doi.org/10.1038/nclimate3089>.
- Page, C.M., 2004: Data rescue in the southeast Asia and south Pacific region: challenges and opportunities. *Bull. Am. Meteorol. Soc.*, **85**, 1483-1490.
- Pal, J., and E. Eltahir, 2015: Future temperature in southwest Asia projected to exceed a threshold for human adaptability. *Nat. Clim. Change*, **6**, 197-200, [doi:10.1038/nclimate2833](https://doi.org/10.1038/nclimate2833).
- Parker, W.S., 2016. Reanalyses and Observations: What's the Difference? *Bull. Am. Meteorol. Soc.*, **97**, 1565–1572, <https://doi.org/10.1175/BAMS-D-14-00226.1>.
- Peterson, T., 2013: *Introduction to Quality Control of Daily Climate Data*.
- Piani, C., Weedon, G.P., Best, M., Gomes, S.M., Viterbo, P., Hagemann, S., Haerter, J.O., 2010: Statistical bias correction of global simulated daily precipitation and temperature for the

- application of hydrological models. *J. Hydrol.*, **395**, 199–215.
<https://doi.org/10.1016/j.jhydrol.2010.10.024>.
- Quesada, B., Vautard, R., Yiou, P., Hirschi, M., Seneviratne, S.I., 2012: Asymmetric European summer heat predictability from wet and dry southern winters and springs. *Nat. Clim. Change*, **2**, 736–741, <https://doi.org/10.1038/nclimate1536>.
- Ramage, C.S., 1968: Role of a tropical “maritime continent” in the atmospheric circulation. *Mon. Wea. Rev.*, **96(6)**, 365-370.
- Risbey, J.S., Lewandowsky, S., Langlais, C., Monselesan, D.P., O’Kane, T.J., Oreskes, N., 2014: Well-estimated global surface warming in climate projections selected for ENSO phase. *Nat. Clim. Change*, **4**, 835–840, <https://doi.org/10.1038/nclimate2310>.
- Rivington M, Matthews K, Buchan K, Miller D, Bellocchi GRussell G. 2013: Climate change impacts and adaptation scope for agriculture indicated by agro-meteorological metrics. *Agrict. Syst.*, **114**, 15-31, DOI: 10.1016/j.agsy.2012.08.003.
- Russo S, Dosio A, Graversen R, Sillmann J, Carrao H, Dunbar M, Singleton A, Montagna P, Barbola PVogt J. 2014: Magnitude of extreme heat waves in present climate and their projection in a warming world. *J. Geophys. Res.: Atmos.*, **119(22)**, 12,500-12,512, DOI: 10.1002/2014jd022098.
- Schmidt, G.A., and Coauthors, 2014: Configuration and assessment of the GISS ModelE2 contributions to the CMIP5 archive: GISS ModelE2 CMIP5 simulations. *Journal of Advances in Modeling Earth Systems*, **6**, 141–184, <https://doi.org/10.1002/2013MS000265>.
- Schiermeier, Q., 2018: Clear signs of global warming will hit poorer countries first. Accessed 31 Jul. 2018, <https://www.nature.com/articles/d41586-018-04854-2>.
- Sherwood SHuber M. 2010: An adaptability limit to climate change due to heat stress. *Proc. Natl. Acad. Sci.* **107(21)**, 9552-9555, DOI: 10.1073/pnas.0913352107.
- Sillmann, J., and Coauthors, 2017: Understanding, modeling and predicting weather and climate extremes: Challenges and opportunities. *Weather and Climate Extremes*, **18**, 65–74. <https://doi.org/10.1016/j.wace.2017.10.003>.

- Sillmann, J., Kharin, V.V., Zhang, X., Zwiers, F.W., Bronaugh, D., 2013a: Climate extremes indices in the CMIP5 multimodel ensemble: Part 1. Model evaluation in the present climate: Climate extremes indices in CMIP5. *J. Geophys. Res.: Atmos.*, **118**, 1716–1733. <https://doi.org/10.1002/jgrd.50203>.
- Sillmann, J., Kharin, V.V., Zwiers, F.W., Zhang, X., Bronaugh, D., 2013b: Climate extremes indices in the CMIP5 multimodel ensemble: Part 2. Future climate projections: CMIP5 projections of extremes indices. *J. Geophys. Res.: Atmos.*, **118**, 2473–2493. <https://doi.org/10.1002/jgrd.50188>.
- Smitha, P.S., Narasimhan, B., Sudheer, K.P., Annamalai, H., 2018: An improved bias correction method of daily rainfall data using a sliding window technique for climate change impact assessment. *J. Hydrol.*, **556**, 100–118. <https://doi.org/10.1016/j.jhydrol.2017.11.010>.
- Stocker T. F., and Coauthors, 2014: *Fifth Assessment Report - Climate Change 2013*. Ipcc.ch.
- SU, H., Neelin, J.D., Meyerson, J.E., 2005: Mechanisms for Lagged Atmospheric Response to ENSO SST Forcing. *J. Clim.*, **18**, 21.
- Sun, Q., Miao, C., Duan, Q., Kong, D., Ye, A., Di, Z., Gong, W., 2014: Would the ‘real’ observed dataset stand up? A critical examination of eight observed gridded climate datasets for China. *Environ. Res. Lett.*, **9**, 015001. <https://doi.org/10.1088/1748-9326/9/1/015001>.
- Supari, Tangang, F., Juneng, L., Aldrian, E., 2017: Observed changes in extreme temperature and precipitation over Indonesia: Extreme temperature and precipitation over indonesia. *Int. J. Climatol.*, **37**, 1979–1997. <https://doi.org/10.1002/joc.4829>.
- Tangang, F.T., Juneng, L., Ahmad, S., 2007: Trend and interannual variability of temperature in Malaysia: 1961–2002. *Theoretical and Applied Climatology*, **89**, 127–141. <https://doi.org/10.1007/s00704-006-0263-3>.
- Tebaldi, C., Hayhoe, K., Arblaster, J.M., Meehl, G.A., 2006: Going to the Extremes: An Intercomparison of Model-Simulated Historical and Future Changes in Extreme Events. *Clim. Change*, **79**, 185–211. <https://doi.org/10.1007/s10584-006-9051-4>.

- Terando, A., Easterling, W.E., Keller, K., Easterling, D.R., 2012: Observed and Modeled Twentieth-Century Spatial and Temporal Patterns of Selected Agro-Climatic Indices in North America. *J. Clim.*, **25**, 473–490. <https://doi.org/10.1175/2011JCLI4168.1>.
- Teutschbein, C., Seibert, J., 2012: Bias correction of regional climate model simulations for hydrological climate-change impact studies: Review and evaluation of different methods. *J. Hydrol.*, **456–457**, 12–29, <https://doi.org/10.1016/j.jhydrol.2012.05.052>.
- Thirumalai, K., DiNezio, P.N., Okumura, Y., Deser, C., 2017: Extreme temperatures in Southeast Asia caused by El Niño and worsened by global warming. *Nat. Commun.*, **8**, 15531. <https://doi.org/10.1038/ncomms15531>.
- Trenberth, K.E., 2012: Framing the way to relate climate extremes to climate change. *Clim. Change*, **115**, 283–290. <https://doi.org/10.1007/s10584-012-0441-5>.
- Trenberth, K., 2011: Changes in precipitation with climate change. *Clim. Res.*, **47**, 123–138. <https://doi.org/10.3354/cr00953>.
- Trenberth, K.E., 2002: Evolution of El Niño–Southern Oscillation and global atmospheric surface temperatures. *J. Geophys. Res.*, **107**, <https://doi.org/10.1029/2000JD000298>.
- Trewin, B., 2014: *The climates of the Tropics, and how they are changing*, 13 pp.
- Vavrus, S., Walsh, J.E., Chapman, W.L., Portis, D., 2006: The behavior of extreme cold air outbreaks under greenhouse warming. *Int. J. Climatol.*, **26**, 1133–1147, <https://doi.org/10.1002/joc.1301>.
- Vecchi, G.A., Wittenberg, A.T., 2010: El Niño and our future climate: where do we stand?: El Niño and our future climate. *Wiley Interdisciplinary Reviews: Climate Change*, **1**, 260–270, <https://doi.org/10.1002/wcc.33>.
- Vincent, L.A., Mekis, É., 2006: Changes in Daily and Extreme Temperature and Precipitation Indices for Canada over the Twentieth Century. *Atmos.-Ocean*, **44**, 177–193, <https://doi.org/10.3137/ao.440205>.
- Visher, S. S., 1922: Variability vs. Uniformity in the Tropics. *The Scientific Monthly*, **1**, 22-34, <http://www.jstor.org/stable/6254>.

- Voltaire, A., and Coauthors, 2013: The CNRM-CM5.1 global climate model: description and basic evaluation. *Clim Dyn.*, **40**, 2091–2121, <https://doi.org/10.1007/s00382-011-1259-y>.
- Wang, X.L., Trewin, B., Feng, Y., Jones, D., 2013: Historical changes in Australian temperature extremes as inferred from extreme value distribution analysis: Trends in australia temperature extremes. *Geophys. Res. Lett.*, **40**, 573–578, <https://doi.org/10.1002/grl.50132>.
- World Bank, 2018: Population, total | Data. Accessed August 6, 2018, <https://data.worldbank.org/indicator/SP.POP.TOTL> ().
- World Meteorological Organization, 1989: *Calculation of Monthly and Annual 30-Year Standard Normals*. WCDP-No. 10, WMO-TD/No. 341, World Meteorological Organization.
- Wu J, Zhou Y, Gao Y, Fu J, Johnson B, Huang C, Kim YLiu Y. 2013: Estimation and Uncertainty Analysis of Impacts of Future Heat Waves on Mortality in the Eastern United States. *Environ. Health Perspect.*, DOI: 10.1289/ehp.1306670.
- Xu, P., Huang, J., Miller, N., Schleger, N., 2009: *Effects of Global Climate Change on Building Energy Consumption and Its Implications On Building Energy Codes and Policy In California*.
- Yin, H., Donat, M.G., Alexander, L.V., Sun, Y., 2015: Multi-dataset comparison of gridded observed temperature and precipitation extremes over China: Temperature and precipitation extremes over China. *Int. J. Climatol.*, **35**, 2809–2827, <https://doi.org/10.1002/joc.4174>.
- Yoshida Y, Maruyama K, Tsutsui J, Nakashiki N, Bryan FO, Blackmon M, Boville BA, Smith RD, 2005: Multi-century ensemble global warming projections using the Community Climate System Model (CCSM3). *J Earth Simulator*, **3**, 2–10.
- Yukimoto, S., and Coauthors, 2012: A New Global Climate Model of the Meteorological Research Institute: MRI-CGCM3 "Model Description and Basic Performance". *J. Meteorol. Soc. Jpn.*, **90A**, 23–64, <https://doi.org/10.2151/jmsj.2012-A02>.
- Zhang, X., and F. Yang, 2004: *RClimDex (1.0) User Manual*. Canada,.
- Zhang, X., Hegerl, G., Zwiers, F.W., Kenyon, J., 2005: Avoiding Inhomogeneity in Percentile-Based Indices of Temperature Extremes. *J. Clim.*, **18**, 1641–1651. <https://doi.org/10.1175/JCLI3366.1>.

Zampieri, M., D'Andrea, F., Vautard, R., Ciais, P., de Noblet-Ducoudré, N., Yiou, P., 2009: Hot European Summers and the Role of Soil Moisture in the Propagation of Mediterranean Drought. *J. Clim.*, **22**, 4747–4758, <https://doi.org/10.1175/2009JCLI2568.1>.

Zhai, F., Zhuang, J., 2012: Agricultural Impact of Climate Change: A General Equilibrium Analysis with Special Reference to Southeast Asia. *Climate Change in Asia and the Pacific: How Can Countries Adapt?* SAGE Publications India, 17–35. <https://doi.org/10.4135/9788132114000.n3>.